

## 11. SITE 879<sup>1</sup>

### Shipboard Scientific Party<sup>2</sup>

#### HOLE 879A

**Date occupied:** 15 July 1992

**Date departed:** 17 July 1992

**Time on hole:** 2.3 days

**Position:** 34°10.46'N, 144°18.56'E

**Bottom felt (rig floor, m; drill-pipe measurement):** 1512.5

**Distance between rig floor and sea level (m):** 11.7

**Water depth (drill-pipe measurement from sea level, m):** 1500.8

**Total depth (rig floor, m):** 1512.5

**Penetration (m):** 226.5

**Number of cores (including cores with no recovery):** 24

**Total length of cored section (m):** 226.50

**Total core recovered (m):** 39.55

**Core recovery (%):** 17.5

**Oldest sediment cored:**

Depth (mbsf): 191.0

Nature: claystone with relict breccia texture

Age: indeterminate

**Hard rock:**

Depth (mbsf): 226.5

Nature: basalt and volcanic breccia (peperite)

**Principal results:** A local pre-site seismic survey was conducted on Takuyo-Daisan (Seiko) Guyot, in the Seiko cluster of seamounts on the Japanese Seamount province. The *JOIDES Resolution* approached the guyot from the east, and a seismic profile was shot parallel to an east-trending ridge along the southern rim of the guyot. Seismic profiling continued as the ship passed south to north across proposed Site Seiko-1, eastward across proposed Site Seiko-2, and finally in a southwest direction leading to the southern margin. Takuyo-Daisan Guyot was the last of five guyots drilled on Leg 144. As a consequence of time constraints, a new site on the southern perimeter ridge was selected from these seismic profiles, from which a suitable acoustic target was identified.

Coring began on 15 July 1992 and was completed on 17 July, after 2.3 days of drilling Hole 879A. Upon completion of the drilling, Hole 879A was logged using the geophysical tool string and the Formation Micro-Scanner (FMS) tool. After obtaining our drilling and logging objectives at Hole 879A, we departed Site 879 on 18 July 1992.

Site 879 is located at 34°10.46'N, 144°18.56'E in a water depth of 1501 m atop the southern ridge of the guyot, at the crosspoint between the east-west and south-north seismic lines. Takuyo-Daisan Guyot is the easternmost guyot of the Seiko cluster of seamounts, in the 30°–35°N guyot band in the northwestern Pacific. The objectives at Site 879 were (1) to determine the genesis of the rough surface topography in relation to the hypothesis of emergence and karsting of the platform limestone cap before the final drowning; (2) to establish the stratigraphy and examine the faunas and floras

of the platform facies and changes with time; (3) to examine the diagenesis of the platform limestones compared with that of the younger guyots drilled in the Marshall Islands; (4) to determine the age and causes of platform drowning, possible emergence, and subsidence history of the atoll limestone relative to sea level; (5) to compare the geological history of Site 879 with that of the other western Pacific guyots drilled during Legs 143 and 144; (6) to establish the age and paleolatitude of the volcanic edifice; and (7) to obtain geochemical data from the volcanic edifice for comparison with other sites and the DUPAL/SOPITA anomaly.

One hole was drilled at Site 879. A reconnaissance of the seafloor was conducted with the vibration-isolated television (VIT); Hole 879A was then spudded on bare rock using the rotary core barrel (RCB). Hole 879A was successfully cored to 226.5 mbsf. The average core recovery was 17.4%, with poor recovery (5.1%) of the platform sequence (four cores with zero recovery). The recovered material included platform limestone (0–150.6 mbsf), argillaceous sandy limestone, calcareous claystone, volcanic conglomerate, calcareous sandstone, and rudstone (150.6–169.7 mbsf), claystone with a relict volcanic texture and minor conglomerates (169.7–190.2 mbsf), and basalt breccia (190.2–226.5 mbsf, total depth [TD]).

A preliminary evaluation of the recovered material at Site 879 yielded three lithologic units. These are based upon a combination of data, including visual core and smear slide descriptions and downhole logging. The age of these units was based mainly on the identification of larger benthic foraminifers and calcareous plankton. The recognized units, from top to bottom are as follows:

Unit I (0–169.7 mbsf) consists of a white, pale brown to brown, sometimes stained, carbonate platform sequence of Albian(?) to late Aptian age. Unit I was divided into five subunits on the basis of depositional texture, variations in the skeletal components, and degree of influx of terrestrial and volcanic materials. Components include gastropods (nerineids and cerithids), bivalves (thin-shelled forms, large oysters, and rudists), corals, benthic foraminifers (orbitolinids, cuneolinids, miliolids), *Ortonella*, dasycladacean algae, oncolids, and peloids; calcisponges and echinoids are minor components. A few intervals in this unit yielded calcareous nannofossils and planktonic foraminifers. Micritization is common. Subunit IA consists of coral-molluscan rudstone and floatstone with a skeletal grainstone to packstone matrix. Subunit IB consists of skeletal packstone and wackestone with rare intervals of grainstone. Intervals with pelagic components are also contained within this subunit. Subunit IC consists of skeletal wackestone with intercalated skeletal packstone; both rock types contain altered basalt lithoclasts of medium-sized sand. Intervals with planktonic foraminifers and nannofossils are also found in this subunit. Subunit ID consists of bioturbated argillaceous limestone, calcareous sandstone, and calcareous claystone intercalated with organic- and clay-rich intervals. An interval several centimeters thick of brown coal, a piece of wood, and fragments of coal incorporated into the calcareous sandstone are contained in this subunit. Subunit ID also contains a volcanic component of altered glass and lithoclasts of basalt; many of the skeletal components are pyritized. Underlying Subunit IE consists of calcareous sandstone, volcanic conglomerate, and gastropod rudstone.

The porosity of the rudstone in Unit I ranges from 1% to 18%, mostly moldic, locally intergranular, and sheltered porosity. The floatstone contains 10%–16%, mostly moldic, solution-enlarged interparticle and intra-particle porosity. The grainstone consists of 2%–15% porosity, of which about 50% is moldic porosity and 50% is intergranular porosity. The packstone has 12%–16% porosity, which includes moldic, solution-enlarged intergranular and possible fenestral porosity. The skeletal pack-

<sup>1</sup> Premoli Silva, I., Haggerty, J., Rack, F., et al., 1993. *Proc. ODP, Init. Repts.*, 144: College Station, TX (Ocean Drilling Program).

<sup>2</sup> Shipboard Scientific Party is as given in the list of participants preceding the contents.

stone, especially in the lower portion, has 1%–5% porosity; it is commonly moldic and vuggy with some intergranular porosity. Porosity is negligible in Subunits ID and IE.

Micronodules, dendrites, and pore linings of manganese are scattered throughout the unit, whereas varicolored grains of altered basalt occur in the lower portion. Only a small fragment of the surficial phosphatic crust (which may have been manganese coated, as noted during the VIT survey) was recovered. The resistivity log registered four plurimetric zones enriched in thorium, which are interpreted to represent clay-rich zones within the host facies of Subunit ID.

Unit II (169.7–191.0 mbsf) consists of clay, claystone with relict volcanic breccia texture, and a minor conglomerate interval that is late Aptian or older in age. Clasts in the breccia are (1) pale yellow, highly vesicular basalt with vesicles filled by zeolite; and (2) dusky red to dark gray basalt with <10% vesicles. The claystone is dark red, dusky red, and reddish black in color, and it displays a relict volcanic breccia texture. The dusky red and reddish black clasts are basalt altered to clay; the matrix is dark red. The dark brown conglomerate is matrix supported and consists of isolated, well-rounded pebbles in a coarse sandy volcanic matrix. Pebbles are orange to yellow brown, highly vesicular aphyric basalt; the pebbles increase in size downward from 0.5–1.0 cm to 1.0–1.5 cm. There is a zonation in the color of some clasts, probably the result of weathering.

Unit III (191.0–226.5 mbsf) consists of 19.5 m of plagioclase phyric basalt intercalated in a complex fashion with volcanic breccia of indeterminate age. This complex intermixture can best be described as a peperite, formed by the intrusion of the basaltic lava into soft, wet sediment. The basalt occurs as irregularly shaped, subspherical, pillow-like bodies, commonly with relict glassy selvages, ranging in size from <1 cm to 1 m or more. The basalt is highly plagioclase phyric with approximately 20% plagioclase (often very fresh in appearance) and minor olivine phenocrysts in a microcrystalline groundmass. The original wet sediment that the basalt “pillows” intruded into is now represented by irregular bodies of volcanic breccia. The breccia is completely altered to clay and/or zeolite minerals, but it still retains the primary textural features in great detail. About 60% of the original clasts are of fragile, angular, highly vesicular, glassy basalt. The remaining clasts are also angular and composed of a variety of nonvesicular basalts, very little of which can be attributed to fragmentation of the associated plagioclase phyric lava. The matrix of the breccia consists of sand-sized shards of the same glassy vesicular basalt as the larger clasts, cemented by bluish green clay or zeolite.

This breccia is very similar in texture to the polymictic breccia of Hole 878A, although it lacks the included limestone clasts. The vesicular clasts are formed from new magma during the eruption, whereas the remainder are fragments of preexisting basalt.

## BACKGROUND AND OBJECTIVES

Takuyo-Daisan Guyot is the easternmost guyot of the Seiko cluster in the Japanese Seamount province, which is in the 30°–35°N guyot band in the northwestern Pacific. Takuyo-Daisan Guyot lies on the M16 lineation with a crustal age of 141 Ma (Nakanishi et al., 1992a, 1992b; Ozima et al., 1977; Vogt and Smoot, 1984). All the guyots in the Japanese Seamounts rise >4500 m above the regional basement. This implies a hotspot-generated swell with a height of 0.5–1 km and an associated thermal resetting of the lithosphere. The age of the volcanism forming the guyot is  $108 \pm 3.4$  Ma, at a paleolatitude of 10°S (Ozima et al., 1977; Vogt and Smoot, 1984); however, a different age and paleolatitude are presented by Sager et al. (in press). Takuyo-Daisan Guyot is interpreted as a guyot characterized by barrier reefs that encircle a deeply eroded volcanic landscape (van Waasbergen and Winterer, in press). The slopes of this guyot are very steep (~21°) and are proposed to be constructed by small lava flows with a low effusive rate during the constructional volcanic phase (Vogt and Smoot, 1984). Sea Beam data show that Takuyo-Daisan Guyot has a central volcano, which projects 110 m above the main summit level, and an outer ridge with an average height of 70 m above the encircled summit (van Waasbergen and Winterer, in press). Seismic profiles show only a

<100-m-thick sequence of possibly lagoonal sediments. Dredge hauls from the southwest flank of the guyot (Heezen et al., 1973) recovered porous bioclastic calcarenites and dense calcilitites, which contain rudists (caprinids), corals, and molluscan fragments of Albian age.

Drilling plans for Takuyo-Daisan Guyot included two sites. The first priority site (proposed Site Seiko-1), was planned to penetrate 50 m into the basement using the rotary core barrel (RCB). Approximately 30 m of pelagic cap and 125 m of carbonate platform (lagoonal section) was anticipated to overlie basement. A second priority site (proposed Site Seiko-2) was also listed for RCB drilling with the aid of a mini-hard-rock guide base (HRB). This second priority site was also planned for 50 m of penetration into basement, but only after coring through potentially 250 m of reef limestone on the perimeter ridge close to the eastern edge of the guyot.

A local pre-site seismic survey over the guyot to select the location of the site was conducted using the 80-in.<sup>3</sup> water gun as the primary acoustic source. The new seismic line shows that, at proposed Site Seiko-1, the acoustic character of the packet beneath the few-meter-thick pelagic cap is suggestive of a volcanoclastic wedge prograding toward the edges of the guyot rather than the anticipated stratified lagoonal sediments. Therefore, in an attempt to acquire a possibly complete platform sequence, the primary site objective was focused on drilling the perimeter ridges. Takuyo-Daisan Guyot was the last of five guyots to be drilled on Leg 144. As a consequence of time constraints, a new site was selected on the seismic profile. Site 879 is located on the southern perimeter ridge, where the inferred depth to the acoustic basement was around 180 m. At proposed Site Seiko-2 on the northern ridge, the sedimentary sequence was much thicker (ca. 250 m); it would have required 2 extra days to drill through these sediments and reach the basement reflector.

The scientific objectives at Site 879 were (1) to determine the genesis of the rough surface topography in relation to the hypothesis of emergence and karsting of the platform limestone before the final drowning; (2) to establish the stratigraphy and examine the faunas and floras of the platform facies and facies changes with time; (3) to examine the diagenesis of the platform limestones compared to the younger guyots drilled in the Marshall Islands; (4) to determine the age and causes of platform drowning, possible emergence, and subsidence history of the carbonate platform relative to sea level; (5) to compare the geological history of Site 879 with that of the other western Pacific guyots drilled during Legs 143 and 144; (6) to establish the age and paleolatitude of the volcanic edifice; and (7) to obtain geochemical data from the volcanic edifice for comparison with other sites and the DUPAL/SOPITA anomaly.

Drilling at Site 879, on Takuyo-Daisan Guyot, recovered platform carbonates, volcanoclastics, clay, and basalt. The primary objectives of this site are addressed with the preliminary shipboard studies and additional shore-based studies.

## OPERATIONS

Takuyo-Daisan Guyot is the largest and easternmost guyot of the Seiko cluster of the seamounts in the Japanese Seamounts. The guyot lies about 190 nmi southeast of Inubo Saki on the main Japanese island of Honshu. The local pre-site survey required just over 5 hr and covered about 31 nmi. The proposed site was crossed early in the survey, and a beacon drop was planned for the second and final crossing. A last-minute problem occurred with the beacon rigging; consequently, the beacon was not ready to launch when the site was crossed. After a correction of the problem, the ship turned and recrossed the site. Beacon launch was at 0339L (L = local time), 15 July 1992 (1839Z).

### Hole 879A

The drill string was made up with a RCB bit and abbreviated “bare-rock” bottom-hole assembly (BHA). While the top drive was

being picked up, the VIT frame was deployed for a seafloor survey and the selection of a spud site.

The seafloor in the selected area was fairly smooth, with essentially no observable microrelief; some areas had a thin blanket of pelagic sediment that obscured the underlying topography. No prominent relief, depressions, or fissures were observed that could be used to restrain the drill pipe laterally during the initial spudding of the hole. After a reconnaissance of about 1.75 hr, the bit was set down 1501 m below sea level, in an area where the outcropping surface of the feature was slightly rough. Motion on the drill string was compensated while the VIT was recovered.

Hole 879A was spudded by applying slow rotation and light weight on the core bit. After a few min, an increase in torque showed that the bit was "biting," and a falloff in applied weight indicated that penetration had begun. The initial 6 m of core recovered required 80 min to cut—a reasonable rate of penetration (ROP) for limestone—but only 24 cm of core was recovered. The pipe began torquing and sticking during the recovery of Core 144-879A-1R. The manner of sticking suggested that rocks were falling into the hole from the seafloor and wedging at the bit. The problem disappeared after a few minutes.

As coring progressed, increasing weight could be applied to the bit as drill collars went into the hole. The typical pattern of drilling in the uppermost sections of limestone on Leg 144 was observed. At about 25 mbsf, the indurated limestone changed drilling character; the ROP increased dramatically as the bit penetrated friable limestone. Core recovery was about 7% over the upper 54 m of Hole 879A (see Table 1); below this, however, three consecutive zero-recovery cores were taken through an interval where the average ROP was 42 m/hr. Although circulating pressure was normal, a bit deplugger was pumped down to ensure that the bit throat was unobstructed. A small amount of core was recovered on the subsequent attempt, but it was accompanied by a decrease in ROP.

Core recovery then averaged about 4% through interbedded, poorly cemented, and well-cemented limestones to about 150 mbsf, where increasing volcanogenic components altered the properties of the sediment and increased the recovery rate. Below a few meters of interbedded limestone and ash, the sediment was composed of breccia containing volcanic debris. The material was highly altered, hard, and waxy, reducing its ability to be drilled as well as the ROP (as low as 2 m/hr in some intervals). Torque began increasing gradually as Core 144-879-21R was being cut, until the top drive stalled and the drill string stuck at 195 mbsf. The circulating pressure remained near normal, but the problem appeared to be clay constricting the borehole. The pipe was worked free and the hole interval immediately above was reamed until torque returned to normal. No further coring problems were encountered. Basalt continued to total depth at 226.5 mbsf, with the ROP increasing as the amount of clayey alteration products decreased. Coring ended short of the desired 50-m volcanic penetration because of limited operating time left in the leg.

After the final core, a routine wiper trip was made to prepare the hole for logging. A clean hole was expected, with the possible exception of tight spots in the clay zones. Considerable drag was experienced as the bit was pulled through the entire hole interval, even in the presumably washed-out limestone sections. The pipe became stuck vertically and rotationally at 62 mbsf for a brief period before it worked free. Drag continued on the down-trip, but only in the upper half of the hole. The clay/volcanic section was clean and only 5 m of fill were found at total depth.

Following a 30-bbl mud sweep, the rotary shifting tool (RST) was run to release the bit with the mechanical bit release (MBR). An apparently routine release was made, but the second run with the RST to downshift the internal sleeve encountered problems. The sleeve could not be shifted down, indicating a possible nonrelease or fouling of the mechanism. Then the RST became stuck in the outer core barrel (OCB) and was freed only after about 0.5 hr of effort. The RST was in good condition when recovered and the downhole anomalies were

**Table 1. Coring summary, Site 879.**

| Core no.      | Date (July 1992) | Time (Z) | Depth (mbsf) | Cored (m) | Recovered (m) | Recovery (%) |
|---------------|------------------|----------|--------------|-----------|---------------|--------------|
| 144-879A-     |                  |          |              |           |               |              |
| 1R            | 15               | 0510     | 0-6.0        | 6.0       | 0.24          | 4.0          |
| 2R            | 15               | 0655     | 6.0-15.5     | 9.5       | 1.50          | 15.8         |
| 3R            | 15               | 0900     | 15.5-25.0    | 9.5       | 0.79          | 8.3          |
| 4R            | 15               | 1000     | 25.0-34.6    | 9.6       | 0.13          | 1.4          |
| 5R            | 15               | 1120     | 34.6-44.3    | 9.7       | 0.76          | 7.8          |
| 6R            | 15               | 1255     | 44.3-53.9    | 9.6       | 0.15          | 1.6          |
| 7R            | 15               | 1320     | 53.9-63.6    | 9.7       | 0             | 0            |
| 8R            | 15               | 1420     | 63.6-73.2    | 9.6       | 0             | 0            |
| 9R            | 15               | 1530     | 73.2-82.9    | 9.7       | 0             | 0            |
| 10R           | 15               | 1735     | 82.9-92.5    | 9.6       | 0.29          | 3.0          |
| 11R           | 15               | 1900     | 92.5-102.1   | 9.6       | 0.22          | 2.3          |
| 12R           | 15               | 2000     | 102.1-111.8  | 9.7       | 0             | 0            |
| 13R           | 15               | 2200     | 111.8-121.5  | 9.7       | 0.04          | 0.4          |
| 14R           | 16               | 0000     | 121.5-131.1  | 9.6       | 0.34          | 3.5          |
| 15R           | 16               | 0240     | 131.1-140.8  | 9.7       | 0.39          | 4.0          |
| 16R           | 16               | 0435     | 140.8-150.4  | 9.6       | 1.25          | 13.0         |
| 17R           | 16               | 0635     | 150.4-160.1  | 9.7       | 2.24          | 23.1         |
| 18R           | 16               | 0915     | 160.1-169.7  | 9.6       | 0.48          | 5.0          |
| 19R           | 16               | 1420     | 169.7-179.4  | 9.7       | 4.83          | 49.8         |
| 20R           | 16               | 1840     | 179.4-188.7  | 9.3       | 8.05          | 86.5         |
| 21R           | 16               | 2345     | 188.7-198.1  | 9.4       | 1.85          | 19.7         |
| 22R           | 17               | 0345     | 198.1-207.6  | 9.5       | 9.32          | 98.1         |
| 23R           | 17               | 0730     | 207.6-217.0  | 9.4       | 5.83          | 62.0         |
| 24R           | 17               | 1045     | 217.0-226.5  | 9.5       | 0.85          | 9.0          |
| Coring totals |                  |          |              | 226.5     | 39.55         | 17.5         |

**Table 2. Well-log data recorded from Hole 879A.**

| Log type                                | Depth (mbsf) |
|---|--------------|
| *Natural gamma ray                      | 0-214        |
| Sonic                                   |              |
| *Neutron porosity (AmBe neutron source) | 38-214       |
| *Lithodensity (Ce gamma-ray source)     | 38-214       |
| Resistivity                             |              |
| Formation MicroScanner                  | 38-214       |

Note: Log data assumes that the seafloor is at 1504.0 m.

\*These logs were recorded in pipe from 0 to 38 mbsf.

unexplained. An additional wireline run with only the sinker bar was made to ensure that the drill string was unobstructed through the bit.

When the end of the pipe had been pulled to logging depth at about 41 mbsf, the logging equipment was rigged and the FMS tool was run into the hole. It reached to within 9 m of total depth and recorded two passes through the hole up to the depth of the pipe. The FMS tool was then exchanged for the geophysical tool string, which found an additional 3 m of hole fill and also logged up to the depth of the pipe. The oversized hole had an adverse effect on the sonic and resistivity logs (see Table 2 for details of the logging program).

When the logging operations were completed, the drill string was pulled clear of the seafloor and the beacon was recovered. As the pipe trip continued, the vessel was offset by global positioning system (GPS) and precision depth recorder (PDR) navigation to locate a suitable site for recovery of the uppermost (pelagic) sediments. The BHA was given an electromagnetic ("magnaflux") inspection as it was recovered.

## UNDERWAY AND SITE GEOPHYSICS

### Introduction

Takuyo-Daisan Guyot, part of the Japanese seamount group, lies ~1000 km north-northwest of MIT Guyot. The edifice is rhombohedral in shape and is centered on 34.2°N latitude and 144.25°E longitude (Fig. 1). According to the magnetic anomaly map of Nakanishi et al. (1992a), Takuyo-Daisan straddles Anomaly M16, making the plate age upon which this edifice is built ~141 m.y. old.

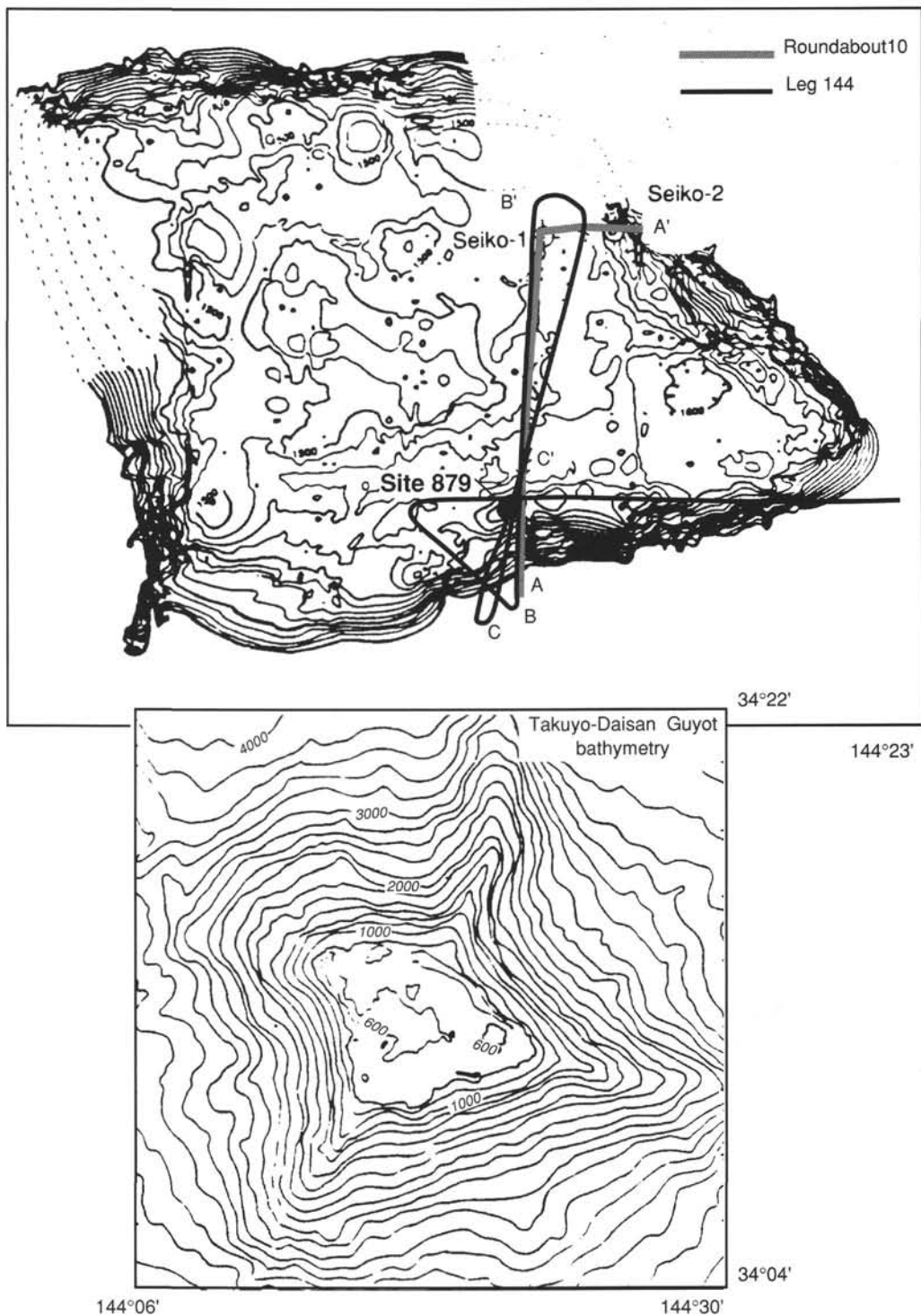


Figure 1. Bathymetry and profile locations over Takuyo-Daisan (Seiko) Guyot. Bathymetric data are from Roundabout Cruise 10, and solid black ship tracks are from the Leg 144 site survey.

#### Site Survey—Roundabout 10

The site survey work over this guyot was done primarily during Leg 10 of the 1988 Roundabout Expedition (hereafter referred to as Roundabout 10) on the *Thomas Washington*. Geophysical data collected over Takuyo-Daisan Guyot includes Sea Beam multibeam bathymetry, 3.5-kHz echo-sounder bathymetry, single-channel seis-

mic records, and gravity and magnetic measurements. Dredges along the flanks of the guyot recovered a mixture of limestone and basalt. The age of the limestone is estimated as mid-Albian to Senonian (J. Grötsch, unpubl. data). Basalts recovered during a previous cruise to this guyot produced an  $Ar/Ar$  age of ~102 Ma (Ozima et al., 1978). From the basalts recovered during Roundabout 10, Sager et al. (in press) calculate a paleopole for Takuyo-Daisan Guyot of 58.2°N

latitude and 144.2°E longitude. This pole is consistent with other poles calculated for the Japanese seamounts, all of which cluster along the 82–125 Ma section of the Pacific Apparent Polar Wander Path.

From the geophysical and geological data collected during Roundabout 10, van Waasbergen and Winterer (in press) discuss the relationship between the summit morphology of Takuyo-Daisan Guyot, among other guyots, and presumed regional tectonic events affecting this area of the Pacific Plate. They provide the following description of Takuyo-Daisan Guyot: the summit has a central volcano, which stands 110 m above the main summit level, and a tall rim along the outer edge of the summit platform. The rim is up to 100 m higher than the summit plateau; it consists of discontinuous segments 600–1000 m wide, which are best developed along the northeast and south sides. The average height of these rim sections is about 70 m above the main summit level. The gaps between rim sections go down to 40 m below the main summit level and appear to have small terraces in front of them, on the lower slopes, at a depth of 1600 m.

Van Waasbergen and Winterer (in press) suggest that both the presence of closed depressions within the “lagoonal” portion of the summit and anomalously tall (80–100 m) reef rims are indicative of karst topography on Takuyo-Daisan Guyot. They postulate that both features result from subaerial exposure and erosion of a more complete carbonate platform that existed on top of the volcanic edifice at one time. Additional evidence cited in support of substantial subaerial exposure includes the presence of channels cutting through the gaps in the rim sections and the occurrence of small (<500 m wide), presumably wave-cut terraces downslope and outside of the perimeter ridges.

Many of the smaller features mentioned in the above paragraph (e.g., terraces, channels, and platform depressions) are not clearly visible in Figures 1 and 2, but these figures represent only a small portion of the entire data base over Takuyo-Daisan Guyot. The seismic profile in Figure 2, collected during Roundabout 10, shows the primary features found across the summit. Along the south flank, a perimeter ridge extends almost 100 m above the seafloor. Basement may be shown by the strong reflector beneath the ridge. In this profile, the central high, presumably volcanic, basement is ~10 m deeper than the south ridge and ~50 m deeper than the north ridge. It is difficult to discern any coherent reflectors much deeper than 2.2 s TWT north of the central basement high, or deeper than 2.28 s TWT along the south flank. No pelagic sediment is visible in Figure 2.

### Site Survey—Leg 144

The survey over Takuyo-Daisan Guyot concentrated on collecting data over the perimeter ridges along the south and north sides of the summit (Fig. 1). Approaching the guyot from the east, we began deploying the seismic gear on Julian Day (JD) 196, around 1420Z (GMT). After the gear was in the water, we began collecting data over the south perimeter ridge on a heading of 274° with a ship's speed of 6 kt and using a 200-in.<sup>3</sup> water gun as a source. At 1545Z the ship changed course to 120°. At about this same time, the digital seismic acquisition system began giving error messages in response to missed shots from the water gun. Addressing this problem, we deployed an 80-in.<sup>3</sup> water gun at 1615Z and recovered the 200-in.<sup>3</sup> water gun. The ship changed course to 000° at 1630Z. After cresting the summit edge, a sonobuoy was launched at 1644Z. The signal received from this buoy was sporadic and relatively weak. Consequently, it is difficult to determine whether the refraction data will be useful; detailed analysis of the data awaits post-cruise processing. Before crossing the north perimeter ridge, the ship looped to the southeast and then turned again to a heading of 210°. At 1804Z the ship passed over the potential site location on the south perimeter ridge. After reversing course, the beacon was dropped at 1839Z on JD 196. This time corresponds to a location of 34°10.33'N latitude and 144°18.50'E longitude. By 1846Z the seismic gear was recovered, and by 1900Z the ship was on station over Site 879.

On the basis of the 3.5-kHz profiles, very little pelagic sediment appears to accumulate across the summit of Takuyo-Daisan Guyot

(Fig. 3). The smooth appearance of the summit seafloor suggests that at least a veneer of pelagic sediment covers the presumably rough platform topography, but a distinct reflector between the two presumed lithologies is not apparent (unlike the guyots in the southern Marshall Islands). Relief on the south perimeter ridge, measured from the top of the ridge to the platform surface behind the ridge, is less than ~82 m. Across the summit, a number of features marked by strong hyperbolic reflectors crop out from the overlying, presumed veneer of pelagic sediments. The central topographic high is the most prominent of these features, and it extends over 40 m above the surrounding platform surface. The perimeter ridge along the north flank of Takuyo-Daisan Guyot is ~50 m high.

Figures 4 and 5 are representative examples of the seismic data collected during Leg 144. Although the quality of the seismic data presented in these figures is not exceptional, additional post-cruise processing may improve the records. The south flank of Takuyo-Daisan Guyot steps down from the top of the perimeter ridge across a number of slope breaks. In Figure 4 the slope breaks occur at 2.45, 2.28, 2.21, and 2.16 s TWT. In Figure 5, the slope breaks occur at 2.50, 2.27, 2.17, and 2.12 s TWT. Two acoustic units compose the perimeter ridge and outer slope along the south flank of Takuyo-Daisan Guyot. A packet of poorly defined reflectors overlies a sequence of stronger reflectors (marked as basement in Fig. 5). The strong reflector packet appears to crop out along the outer slope at ~2.5 s TWT. The ridge beneath Site 879 may thus consist of a packet of sediments 0.20 s TWT thick overlying volcanic basement.

The central topographic high may represent a local shallowing of the volcanic basement. It lies 2.2 km behind the south perimeter ridge. A series of prograding reflectors extends 2.5 km to the north of the basement high. Beyond this distance, the reflector packet becomes more hummocky and less defined. If the prograding unit is similar to the one drilled on Limalok Guyot, then it could represent a sequence of volcanoclastic sediments building outward from the central basement high. The acoustic unit overlying the last prograding reflector reaches a maximum thickness of 0.11 s TWT in Figure 4.

## LITHOSTRATIGRAPHY

The RCB system was used to drill one hole (Hole 879A) at Takuyo-Daisan Guyot (Site 879). Total depth of penetration was 226.5 mbsf. Overall core recovery averaged 17%; however, it averaged <5% in the platform limestone. The definition of the lithologic units is obviously hampered by such low core recovery and by the preliminary state of investigations. Rock types have been identified at the hand-sample scale only. Nevertheless, a few lithologic units and subunits were identified, based on such characteristics as color, carbonate and clay content, fossil and particle constituents, lithification, and sedimentary structures.

The three major lithologies identified at this site are platform carbonates, argillaceous limestones, and sandstones (Unit I, 0–169.7 mbsf), claystone with relict volcanic breccia texture (Unit II, 169.7–191.0 mbsf), and basalt (Unit III: 191.0–226.5 mbsf). Lithologic units and subunits are described below and summarized in Figure 6 and Table 3.

### Unit I

Interval: Core 144-879A-1R to Section 144-879A-19R-1, 0 cm  
Depth: 0–169.7 mbsf  
Age: late Aptian to Albian

Unit I consists of 169.7 m of platform carbonates, argillaceous sandy limestones, and sandstones. Five subunits are defined from this sequence. These are discussed in detail below.

#### Subunit IA

Interval: Core 144-879A-1R to Section 144-879A-6R-1, 0 cm  
Depth: 0–44.3 mbsf  
Age: Albian

Subunit IA consists of 44.3 m of coral-molluscan rudstone and floatstone, skeletal grainstone and packstone, and minor wackestone. In the interval between 0 and 44.3 mbsf, recovery averaged 7% (see "Operations" section, this chapter).

The rudstone of Subunit IA is white (10YR 8/2) to very pale brown (10YR 6/3 and 10YR 8/3 to 8/2). Gastropods (nerineids and cerithids) and bivalve shell fragments are abundant, up to 2 cm and frequently bored, probably by sponges. Bivalves include small thin-shelled forms, thick-walled oysters (e.g., Intervals 144-879A-2R-1, 23–28 cm, 69–78 cm, 95–104 cm, and 129–150 cm), and probable fragments of the compact layer of radiolitic rudists. The matrix is a peloidal skeletal grainstone, fine to coarse grained, with well-rounded grains. Components include peloids, common bivalves, and cyanobacterial bushes (*Ortonella*; e.g., Interval 144-879A-1R-1, 0–11 cm), many gastropods, and green algae (well-preserved dasycladaceans in Interval 144-879A-2R-1, 19–23 cm). Benthic foraminifers (mostly orbitolinids) are frequent (e.g., Interval 144-879A-3R-1, 79–84 cm). Coral fragments are absent to abundant (e.g., Interval 144-879A-2R-1, 55–58 cm); fragments of calcisponges, echinoids, and fish teeth are rare.

Most grains have a micrite envelope and are usually coated by micrite (e.g., Intervals 144-879A-1R-1, 15–19 cm, and -2R-1, 89–95 cm; Fig. 7); large gastropods and bivalve shell fragments have a micritized periphery up to 1 mm thick. Manganese(?) staining and micronodules occur in some molds (Interval 144-879A-1R-1, 21–29 cm); many manganese microdendrites occur adjacent to pores. Brownish yellow stains (10YR 6/6) on shells and internal sediments are probably phosphate (Interval 144-879A-2R-1, 55–64 cm). In this rudstone, porosity ranges from 1% to 18%, mostly moldic; other locally important porosity types are intergranular and shelter. Intergranular pores and borings are locally filled by very pale brown (10YR 8/3), fine peloid packstone. Calcite cements are mostly bladed ( $PB_3C$ ) in intergranular and moldic pores; isopachous, inclusion-rich, fibrous crusts ( $PF_3C$ ) are observed in Interval 144-879A-2R-1, 59–64 cm. Sparse intragranular cement is bladed ( $PB_5C$ ).

Bivalve coral floatstone in a matrix of peloid skeletal wackestone to packstone occurs in Intervals 144-879A-2R-1, 0–5 cm and 14–26 cm, -4R-1, 0–9 cm, and -5R-1, 23–27 cm. The color is white (N9, 10YR 8/1 to 8/2) to yellowish gray (5Y 8/1). Corals range in size from 1 to 7 cm; a few of the corals are bored and encrusted. Bivalves include thin-shelled forms, oysters (up to 7 cm long by 6 cm wide) and few probable rudist fragments. Other skeletal components include many cyanobacterial bushes (*Ortonella*), rare gastropods (nerineids) and benthic foraminifers (orbitolinids, miliolids), and very rare green algae (dasycladaceans). Micritization of grains is extensive; coated grains are abundant in the matrix. In Interval 144-879A-5R-1, 23–27 cm, oncoids are abundant and average 0.6 mm in size, but some of them are as large as 2 cm; the nuclei of oncoids consist mostly of cyanobacterial bushes (*Ortonella*) and bivalve fragments. Black rounded manganese (?) micronodules, less than 0.2 mm in diameter, are rare; yellowish brown (10YR 5/4) microdendrites, possibly phosphatic, occur in pores or may partly replace some grains. Porosity ranges from 10% to 16% and is mostly moldic, solution-enlarged interparticle, and solution-enlarged intraparticle. Calcite cement is rare, mostly bladed ( $PB_3C$ ), and locally stained grayish orange (10YR 7/4); equant calcite cement crusts ( $PE_4C$ ) also occur.

The grainstone of Subunit IA is poorly sorted, with grain sizes varying from fine to coarse sand; grains are well rounded. The color is white (10YR 8/1) to very pale brown (10YR 7/3). Components include abundant peloids and benthic foraminifers (orbitolinids, *Cuneolina*, miliolids, uniserial and biserial forms), many bivalves (including probable fragments of rudists) and gastropods, few cyanobacterial bushes (*Ortonella*); fragments of calcareous sponges, corals, and green algae (dasycladaceans) are rare. Intraclasts of foraminifer wackestone are observed in Interval 144-879A-5R-1, 45–52 cm. Most grains are coated by micrite but micrite envelopes are also prevalent. Typical oncoids, as large as 0.5 cm in size, are observed in Interval 144-879A-5R-1, 31–81 cm (Fig. 8). Yellowish brown (10YR 5/4) microdendrites

occur in pores or may partly replace grains. Porosity ranges from 2% to 15%; about 50% of the porosity is moldic and 50% is intergranular. Calcite cement is coarsely crystalline bladed ( $PB_3C$ ) and equant. Some of the cements have a slight manganese stain (e.g., flecks on pore walls and microdendrites at pore margins).

Packstone of Subunit IA is white (N9 to 10YR 8/1) to very pale brown (10YR 7/3). Skeletal components include abundant to many bivalve fragments, frequently bored, and rare calcareous sponges and peloids. Grains are micritized and commonly coated by micrite. Small (<0.1 mm), black, round manganese(?) micronodules are rare; minor manganese stains occur in pores. Lined burrows, 0.5 to 1 mm size, occur in Interval 144-879A-3R-1, 29–34 cm. Interval 144-879A-3R-1, 86–98 cm, includes extensive encrustation by small clustered irregular calcite chambers and possibly tubes, reminiscent of the *Bacinella* structure. Porosity varies from 12% to 16% and includes moldic, solution-enlarged intergranular and possible fenestral pores. Calcite cement is few, mostly bladed ( $PB_3C$ ).

Wackestone is a minor lithology of Subunit IA and occurs in Interval 144-879A-5R-1, 0–8 cm. Its position in this interval, however, is highly questionable as it occurs only in two drilling pebbles located at the top of Core 144-879A-5R-1. In Interval 144-879A-5R-1, 0–3 cm, the wackestone is capped by a 0.5-cm-thick silicified and phosphatic crust; silt-sized sediments overlying this crust contain Eocene nannofossils (see "Biostratigraphy" section, this chapter). The color of the wackestone is white (10YR 8/1 to 8/2). Components of this wackestone include oncoids, 0.5–1.0 cm in size, peloids, fragments of oysters, small thin-shelled bivalves, small gastropods, and rare coral fragments. Fenestrae are reported in Interval 144-879A-5R-1, 0–3 cm, and consist of small tubules. Porosity ranges from 5% to 10%, and is mostly intergranular to vuggy.

### Subunit IB

Interval: Sections 144-879A-6R-1 to -16R-1, 0 cm  
Depth: 44.3–140.8 mbsf  
Age: late Aptian to Albian

In the interval between 44.3 and 140.8 mbsf, the recovery averaged 1.3% with no recovery in Cores 144-879A-7R to -9R, or in Core 144-879A-12R (see "Operations" section, this chapter). Subunit IB is comprised of 96.5 m of skeletal packstone, wackestone, and grainstone, with minor rudstone. When recovered, the contact between skeletal wackestone and packstone is undulate.

Skeletal packstone is very fine to fine grained; sorting is poor to moderate (i.e., 40–350  $\mu$ m range, with a few larger clasts). The color is white (10YR 8/2) to very pale brown (10YR 7/3 to 6/3). Constituents include many benthic foraminifers (mostly miliolids, textulariids, and coiled, planispiral forms), possible spicules, cyanobacterial bushes (*Ortonella*) and many unidentified skeletal fragments. Large clasts are molluscan shells and molds (including bivalves and nerineid gastropods), and oncoids, some with molluscan fragments and whole gastropods as nuclei. A coral colony occurs in Interval 144-879A-10R-1, 0–6 cm. In Interval 144-879A-13R-1, 0–4 cm, elongate black flecks, 5–40  $\mu$ m, may be manganese or organic carbon but appear metallic. Porosity ranges from 5% to 10% and is mostly moldic, intergranular to vuggy. Cement is mostly fine to medium bladed and equant crusts, some clear and some amber to yellow. Moldic pores and burrows are stained yellow (10YR 7/6), possibly by phosphate, and contain 0.35 mm manganese micronodules. In Interval 144-879A-14R-1, 17–24 cm, thin, abundant, and unoriented fenestrae, are lined with fine, clear, equant calcite.

Skeletal wackestone of Subunit IB occurs in Intervals 144-879A-6R-1, 0–9 cm, -6R-1, 15–19 cm, -10R-1, 6–11 cm, and -14R-1, 0–4 cm. The color is white (10YR 8/1 to 8/2). Components include many benthic foraminifers (*Cuneolina*, *Vercorsella*, textulariids), few to many cyanobacterial bushes (*Ortonella*), leached fragments of bivalves and gastropods, and rare green algae (dasycladaceans). Fenestrae are few and consist of small tubules. Burrows, up to 5 mm in

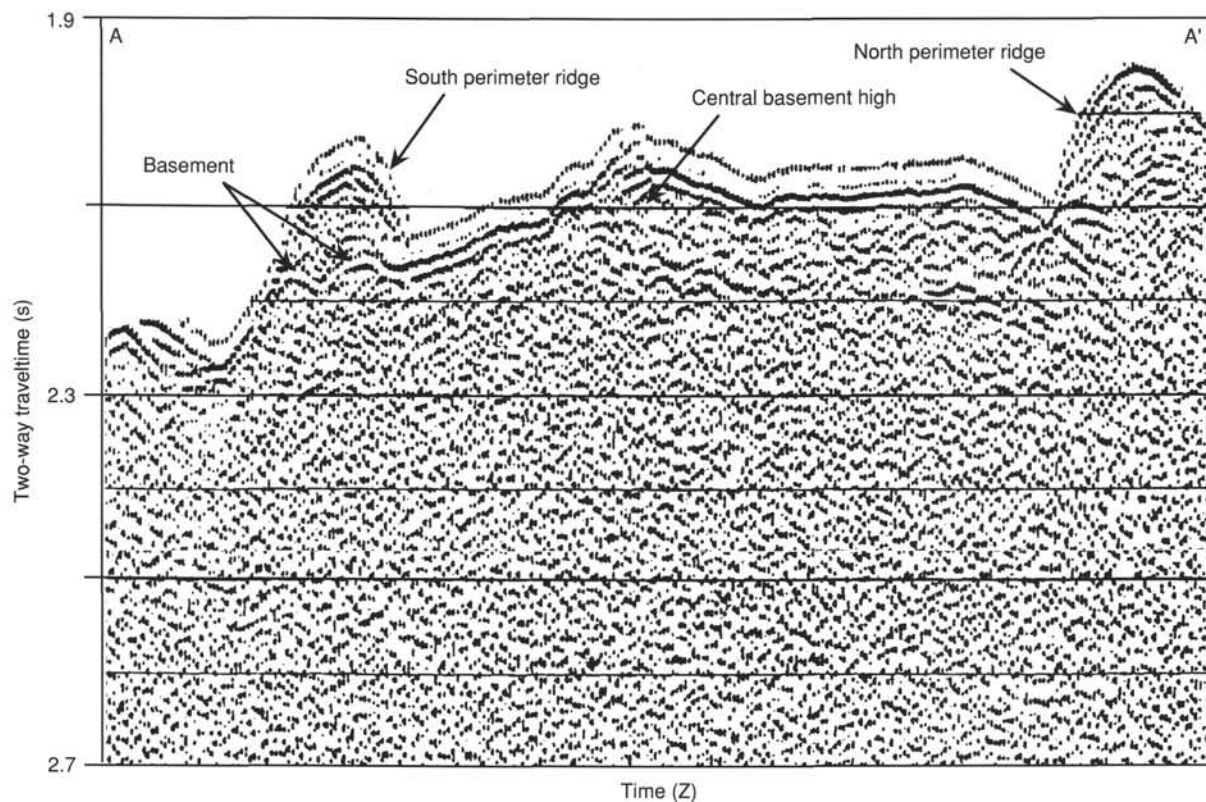


Figure 2. Single-channel seismic Profile A–A' collected during Roundabout Cruise 10, illustrating the primary features associated with Takuyo-Daisan Guyot. Coherent reflectors are difficult to discern much below the seafloor. Profile A–A' location is shown in Figure 1.

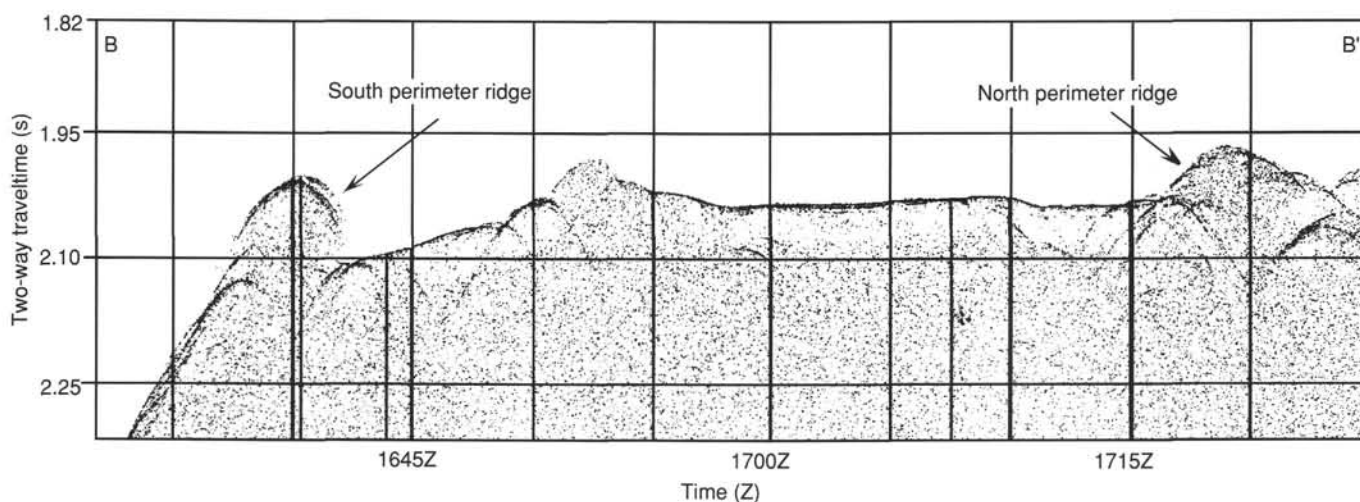


Figure 3. Profile B–B' of 3.5-kHz profile across Takuyo-Daisan Guyot. Profile B–B' location is shown in Figure 1.

diameter, are filled with peloid packstone. Porosity ranges from 1% to 5% and is mostly moldic to vuggy; most vugs are less than 0.15 mm in size (Fig. 9).

Skeletal grainstone of Subunit IB occurs in Intervals 144-879A-6R-1, 12–15 cm, -6R-1, 19–23 cm, and -10R-1, 11–32 cm. Sorting is poor and grain sizes range from fine to coarse sands, with large intraclasts to 2 mm. Grains are well rounded. The color is white (10YR 8/2). Components include benthic foraminifers (miliolids, textulariids, *Cuneolina*), cyanobacterial bushes (*Ortonella*), fragments of gastropods, bivalves (including oysters), and corals. Grains are extensively micritized and coated by micrite. A lithoclast of fenestral wacke-

stone is reported in Interval 144-879A-10R-1, 16–20 cm. In this skeletal grainstone, the porosity ranges from 3% to 15% and is mostly intergranular and vuggy. Calcite cement crusts in intergranular pores are isopachous and bladed (PB<sub>3</sub>C).

Intervals 144-879A-11R-1, 5–23 cm (Fig. 10), -14R-1, 4–8 cm, and 14R-1, 24–37 cm, are comprised of skeletal rudstone. The color is white (10YR 8/2). The rudstone is moderately sorted. Components include small gastropods (especially nerineids), various ornamented bivalves (possibly some rudists), and worm tubes; corals are rare (e.g., Interval 144-879A-14R-1, 37–41 cm). Some of the molluscan shells and whole gastropods are as large as 4 cm in size and have isopachous

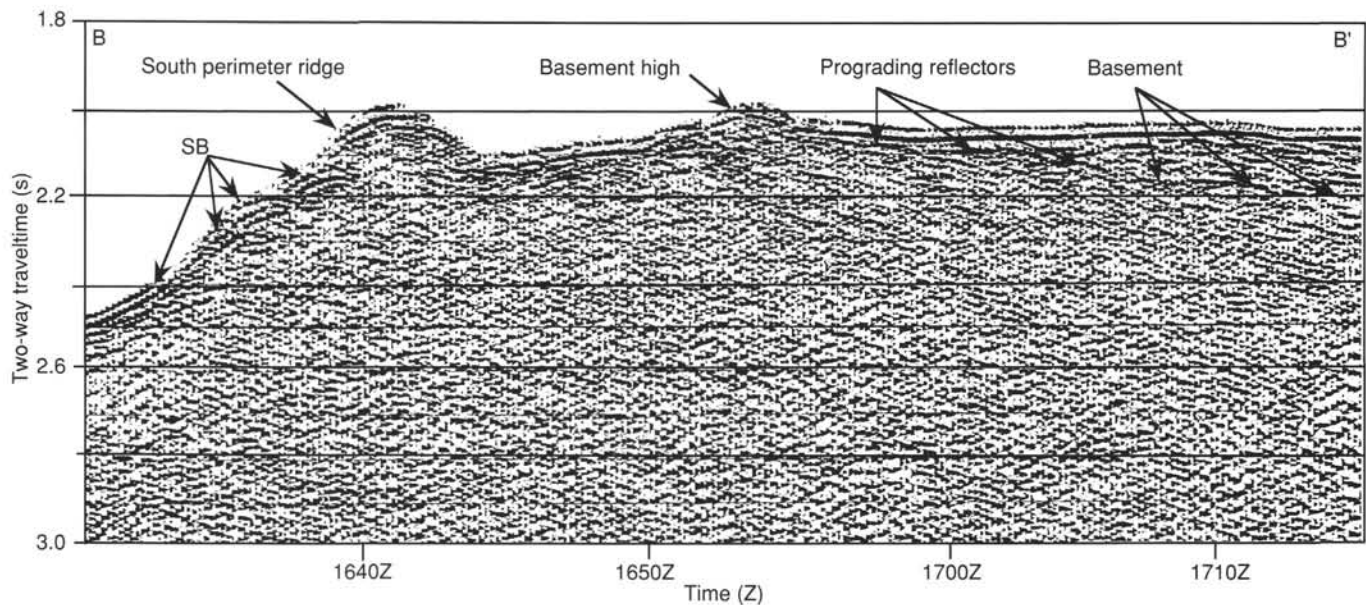


Figure 4. Single-channel seismic Profile B–B' collected during Leg 144. Profile B–B' location is shown in Figure 1. SB = slope breaks down from the perimeter ridge.

micritic coatings as thick as 2 mm. The matrix is composed of fine-grained peloid grainstone, and it includes a few foraminifers (*Vercorsella* and possible *Orbitolina*) and rare cyanobacterial bushes (*Ortonella*). Burrows, up to 1.5 cm in cross section, are reported in Interval 144-879A-14R-1, 24–37 cm; the surfaces of these burrows are stained gray, and the burrows are filled by a very pale brown (10YR 8/3) fine packstone. Porosity averages 7% and is primarily intergranular; moldic porosity is developed after molluscan shells and may be filled by peloid packstone. Cement crusts of clear to amber, bladed calcite (PB<sub>3</sub>C) occur in intergranular pores.

#### Subunit IC

Interval: Sections 144-879A-16R-1 to -17R-1, 18 cm  
Depth: 140.8–150.6 mbsf  
Age: late Aptian

Subunit IC consists of skeletal wackestone (Fig. 11) and minor intervals of skeletal packstone; red (10R 4/6), moderate blue (5BG 4/6), and gray (N6) grains of altered basalt are common in both lithologies.

The wackestone is variably colored: light gray (10YR 7/1), gray (N4 and N5), yellow (10YR 7/6), and light yellowish brown (2.5Y 6/4). Common components include small thin-shelled bivalve fragments, small gastropods (leached or recrystallized), benthic foraminifers (textulariids and miliolids), and fragments of rudists (usually the compact layer of radiolitids). Stromatoporoid and coral fragments are present but less common. Some grains are micritized and coated by micrite (e.g., Interval 144-879A-16R-1, 3–68 cm); bivalve fragments are occasionally recrystallized and well rounded (e.g., Interval 144-879A-16R-1, 68–94 cm). Some burrows are filled by coarse packstone sediment (e.g., Interval 144-879A-16R-1, 3–10 cm); others are stained yellow or infilled by yellowish brown (10YR 5/6) or light olive gray (5Y 6/2), argillaceous and silt-sized sediment. The wackestone matrix may be partly argillaceous. Black, dendritic, manganese accretions occur around cavities in Interval 144-879A-16R-1, 73–79 cm. Visible pyrite is abundant in Interval 144-879A-16R-1, 96–131 cm, as scattered grains, irregular laminae, and in cavities; disseminated, fine-grained pyrite may be responsible for the gray color elsewhere in the subunit.

The intervals of white (10YR 8/2) or very pale brown (10YR 8/3 and 10YR 7/4) skeletal packstone have common red (2.5 YR 5/8) or

reddish yellow (5 YR 6/8) patches and stains, especially at the edge of moldic cavities. Components include abundant oncoids, gastropod fragments, abundant bivalve fragments (including rudists), common peloids, common benthic foraminifers (miliolids, textulariids, and *Vercorsella*), and a few echinoids. Grains are micritized and coated by micrite. Some bored coral fragments form the nuclei to oncoids. Porosity in the packstone ranges from 1% to 5% and is most commonly moldic and vuggy with some intergranular pores.

#### Subunit ID

Interval: Sections 144-879A-17R-1, 18 cm, to -17R-2, 0 cm  
Depth: 150.6–151.9 mbsf  
Age: late Aptian

Light gray (5Y 7/1) to very dark gray (2.5YR N3), burrowed, argillaceous limestone, containing abundant small volcanic grains and woody fragments, constitutes most of Subunit ID, which is only 1.32 m thick. It includes 0.26 m of argillaceous sandstone similar to those in Subunit IE, which also contains volcanic grains and woody material.

The limestone of Subunit ID is argillaceous wackestone (Intervals 144-879A-17R-1, 18–40 cm, and -17R-1, 93–150 cm) and skeletal packstone (Fig. 12) of similar composition, in Interval 144-879A-17R-1, 40–67 cm. In the wackestone, carbonate content averages 74.8% and total organic carbon content is 0.38% (see "Organic Geochemistry" section, this chapter). The color of this limestone varies from very dark gray (2.5YR N3) through dark gray (2.5YR N4 and 5Y 5/1) to gray (2.5YR N5). Skeletal components are bivalves, small gastropods, foraminifers, cyanobacterial bushes (*Ortonella*), and many coral fragments in Interval 144-879A-17R-1, 40–67 cm. Other grains are rounded or recrystallized beyond ready recognition. Thin-shelled bivalves, some articulated, are abundant; the few thicker fragments may include radiolitid rudists (e.g., Interval 144-879A-17R-1, 40–67 cm).

Foraminifers are rare and include textulariids (Interval 144-879A-17R-1, 40–67 cm) and planktonic foraminifers (see "Biostratigraphy" section, this chapter). Volcanic particles are moderate blue-green (5BG 4/6) and red (2.5YR 5/8) grains, are less than 1 mm in diameter, and have dark flakes that are probably volcanic glass. Pyrite has replaced some of the abundant fragments of woody material as well as micrite envelopes and coatings on grains. Bioturbation or distinct burrow mottles about 7 mm in diameter occur throughout with a con-

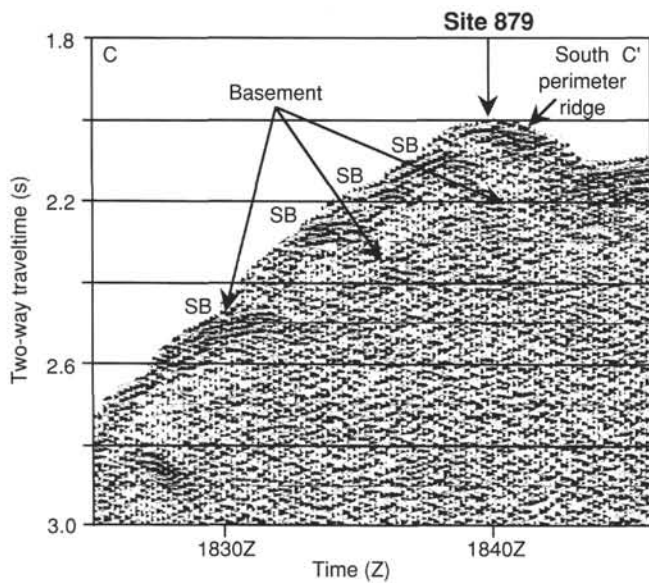


Figure 5. Single-channel seismic Profile C-C' collected during beacon-drop line. Although it is difficult to see in this figure, the horizon marked "Basement" consists of a relatively stronger packet of reflectors than the overlying unit. Profile C-C' location is shown in Figure 1. SB = slope breaks down from the perimeter ridge.

spicuous olive (5Y 5/3) mottling in Interval 144-879A-17R-1, 117-150 cm. Porosity is confined to infilled skeletons and vugs in the packstone (Interval 144-879A-17R-1, 60-62 cm).

The argillaceous sandstone occurs in Interval 144-879A-17R-1, 67-150 cm (Fig. 13). In this argillaceous sandstone, carbonate content varies from 17.5% (Interval 144-879A-17R-1, 74-75 cm) to 5.5% (Interval 144-879A-17R-1, 91-95 cm); sulfur content averages 2.8%; and total organic content averages 1.35% (see "Organic Geochemistry" section, this chapter). This argillaceous sandstone contains many bivalves and a probable coral fragment. Volcanic particles, woody fragments, and pyrite are abundant and similar to that in the limestone. Volcanic particles increase in abundance in Interval 144-879A-17R-1, 80-93 cm. Grain size variations and layers of oriented bivalve fragments produce some stratification despite the presence of burrows expressed as gray lenses that contain considerable carbonate. The typical color of this argillaceous sandstone is black (2.5YR N2.5/0).

**Subunit IE**

Interval: Sections 144-879A-17R-2 to -19R-1, 0 cm  
 Depth: 151.9-169.7 mbsf  
 Age: late Aptian to indeterminate

Subunit IE consists of 17.8 m of volcanic conglomerate and calcareous sandstone. Rudstone occurs in Intervals 144-879A-17R-2, 88-99 cm, and -18R-1, 0-18 cm. The volcanic conglomerate in Subunit IE contains subrounded to well-rounded clasts, as large as 2 cm. Clasts are various shades of gray. Some of the clasts may be sedimentary (probably rare) or deeply weathered volcanic material. The matrix is a mixture of unidentified carbonate and volcanic particles, including pyroxene crystals. Unbroken or slightly crushed bivalve shells and gastropod molds are many. Burrow mottles, about 1 cm wide, are found in zones with lower clast concentrations. A subangular, carbonate-rich domain may be a clast (essentially recycled matrix) or it may be a deformed burrow. The matrix is gray (10YR 5/1) with mottles of light gray (10YR 6/1). Otherwise, grain size and composition are varied.

The dark gray (10YR 4/1) calcareous sandstone in Subunit IE contains varying percentages of pebbles, never greater than 5%, and

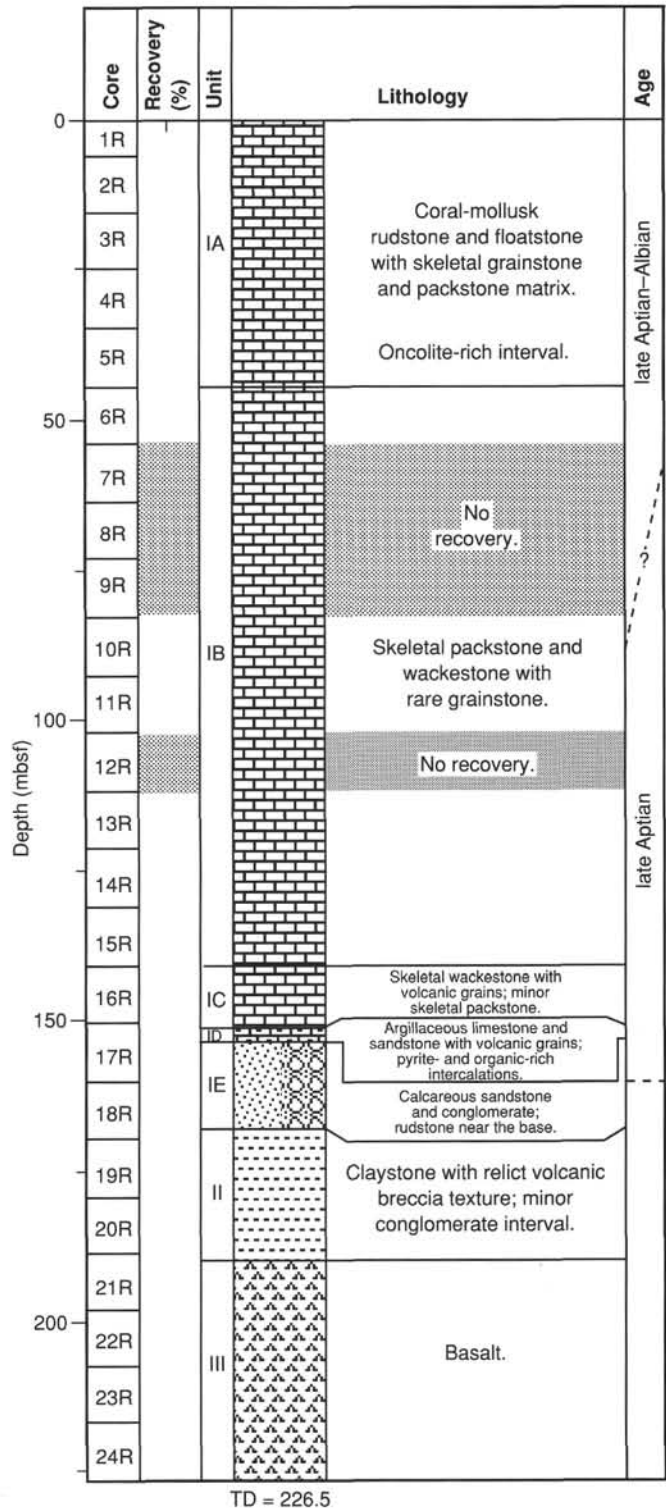


Figure 6. Lithostratigraphic summary of Site 879.

carbonate. Grain size is variable. A lenticular, medium-grained sandstone to siltstone occurs at Interval 144-879A-17R-2, 21-37 cm (Fig. 14). This calcareous sandstone contains altered basalt pebbles, skeletal grains and carbonate-rich lenses. Burrow mottles, many flattened, are observed. The many bivalve fragments that occur in this sandstone include thick-walled and encrusting types. Many of the bivalve shells are compacted and, in some cases, are broken. Several steinkerns of low-spired, smooth gastropods (some as large as 30 mm) are also

**Table 3. Summary of lithostratigraphic units, Site 879.**

| Unit/subunit | Sample numbers                           | Depth (mbsf) | Thickness (m) | Age                          | Lithology   |
|--------------|--|--------------|---------------|------------------------------|---|
| Unit I       | 144-879A-1R-1, 0 cm, to -19R-1, 0 cm     | 0–169.7      | 169.7         | late Aptian–Albian           | Platform carbonate and argillaceous sandy limestones.   |
| Subunit IA   | 144-879A-1R-1, 0 cm, to -6R, 0 cm        | 0–44.3       | 44.3          | late Aptian–Albian           | Coral-mollusk rudstone/floatstone and skeletal grainstone/packstone.  |
| Subunit IB   | 144-879A-6R-1, 0 cm, to -16R-1, 0 cm     | 44.3–140.8   | 96.5          | late Aptian–Albian           | Skeletal packstone and wackestone.  |
| Subunit IC   | 144-879A-16R-1, 0 cm, to -17R-1, 18 cm   | 140.8–150.6  | 9.8           | late Aptian                  | Skeletal wackestone and volcanic grains; minor skeletal packstone.  |
| Subunit ID   | 144-879A-17R-1, 18 cm, to 17R-2, 0 cm    | 150.6–151.9  | 1.3           | late Aptian                  | Argillaceous limestone and argillaceous sandstone with volcanic grains; pyrite- and organic-rich intervals. |
| Subunit IE   | 144-879A-17R-2, 0 cm, to -19R-1, 0 cm    | 151.9–169.7  | 17.8          | late Aptian to indeterminate | Volcanic conglomerate and calcareous sandstone; rudstone near the base.                                     |
| Unit II      | 144-879A-19R-1, 0 cm, to -21R-2, 76 cm   | 169.7–191.0  | 21.3          | Indeterminate                | Claystone with relict volcanic breccia texture; minor conglomerate interval.                                |
| Unit III     | 144-879A-21R-2, 76 cm, to -24R-1, 105 cm | 191.0–226.5  | 35.5          | Indeterminate                | Basalt.   |

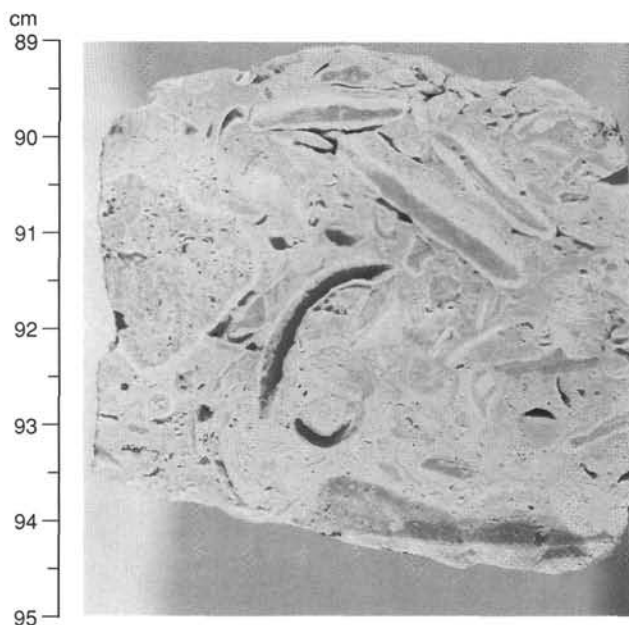


Figure 7. Close-up core photograph of molluscan rudstone typical of the lithology of Subunit IA (Interval 144-879A-2R-1, 89–95 cm). Note that most grains are coated by micrite.

observed. A wavy contact, with 2 cm relief, marked by drape and a coarse sand lens above, occurs at Interval 144-879A-17R-2, 36–38 cm. A dense, calcareous, very fine grained sandstone occurs at Interval 144-879A-17R-2, 37–48 cm. This sandstone has fewer pebbles, skeletal fragments, and burrows than the overlying calcareous sandstone. A coarse-grained, mottled calcareous sandstone occurs at Interval 144-879A-17R-2, 48–76 cm. This sandstone has volcanic clasts (~4%), pyrite, carbonized plant fragments, cylindrical pellets (shrimp pellets?), bivalves (rare), and gastropods (none below Section 144-879A-17R-2, 56 cm).

Other notable features of this subunit include the following:

1. Subangular basalt clasts at Interval 144-879A-17R-2, 67–74 cm. The basalt is coarse grained with feldspar laths and pyroxenes. Pyrite is abundant. The lower clast has strong planar fabric from wavy, discontinuous fractures, with a weakly developed fracture set at ~30° to the main set.

2. Very dark gray (10YR 3/1), carbonaceous, very fine sandstone, with rock fragments less than 2 mm in size, at Interval 144-879A-17R-2, 74–76 cm; and

3. Two coral heads, 60 mm in diameter, at Interval 144-879A-17R-2, 76–88 cm; these were probably clasts in the sandstone.

Peripheral polyps of the coral are filled with silt. Coral margins are deeply etched and blackened, probably by pyrite. Coarse-bladed spar calcite (PB<sub>5</sub>C) cement is leached and fills part of the coral.

White (10YR 7/2) to gray (10YR 5/1) intraclast coated-grain rudstone occurs in Interval 144-879A-17R-2, 88–99 cm. The matrix is silty packstone that contains very poorly sorted, rounded, fine sand particles. Other particles include mollusks, coated grains, possibly echinoderms, and peloids. Coatings are up to 1 mm thick, micritic and unlaminated. Nuclei are fragments of bivalves, calcisponges, corals, and intraclasts. Intraclasts are identical to the matrix. Intraclasts and large coated grains are rimmed by pyrite in the adjacent matrix. Porosity is moldic and ranges from 2% at the top of the interval to 30% at the base. Bladed, coarsely crystalline calcite (PB<sub>4.5</sub>C) cement crusts line molds.

The remaining lithologies of Subunit IE are 18 cm of gastropod rudstone (Interval 144-879A-18R-1, 0–18 cm; Fig. 15) and 32 cm of calcareous sandstone. The former is very pale brown (10YR 7/4) and is extensively bioturbated. Gastropod molds, including nerineids, are common. Most large gastropods are coated by micrite and encrusted by worms? and foraminifers. Holes, probably solution-enlarged burrows, also occur in the rudstone. Burrows also form mottles in this matrix. Dark-gray lime mud lines the walls of these holes and comprises the adjacent carbonate. Some of the burrows are coated by a thin, greenish, soft layer of sediment. Leaching of gastropod shells results in solution-enlarged intraparticle or moldic porosity that averages 15%. The matrix is composed of skeletal peloid packstone. Very few grains are discernable in the matrix. The calcareous sandstone is gray (10YR 6/1), medium-grained, clay-rich, friable, and highly bioturbated. The sandstone is comprised of a mixture of abundant volcanic grains, carbonate grains, coal-rich grains, and unidentifiable black minerals. The matrix is a silt-sized mixture of clay, volcanic, and carbonate grains.

## Unit II

Interval: Sections 144-879A-19R-1 to -21R-2, 76 cm

Depth: 169.7–191.0 mbsf

Age: indeterminate

Unit II consists of 21.3 m of clay, volcanic breccia, and claystone with relict volcanic breccia texture. A minor conglomeratic interval also occurs in Unit II (Interval 144-879A-21R-1, 0–66 cm).

The clay in Unit II occurs at Intervals 144-879A-19R-1, 0–18 cm, and -19R-1, 53–95 cm. Volcanic clasts and pyrite occur in the clay. Pyrite is especially prominent at the top of Section 144-879A-19R-1. The volcanic clasts are plagioclase phyric basalt with 3% of plagioclase.

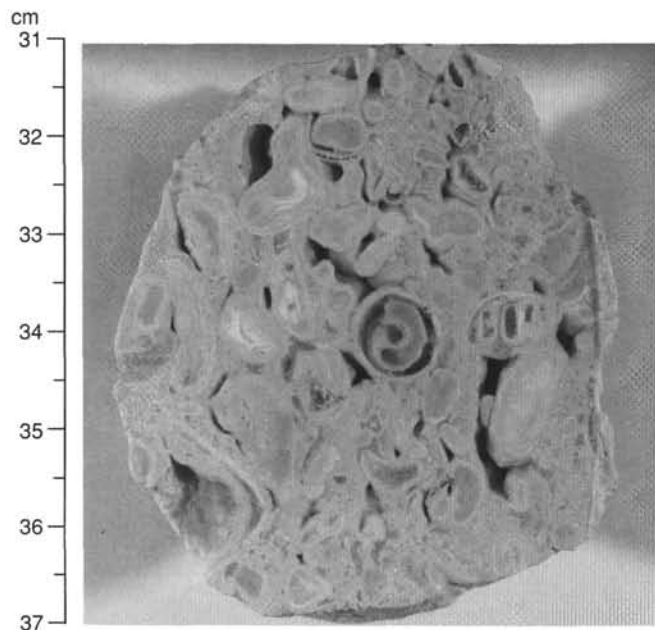


Figure 8. Close-up core photograph of skeletal oncolite floatstone from Subunit IA (Interval 144-879A-5R-1, 31–37 cm). Nuclei of oncolites consists of bivalve fragments and *Ortonella*. The cortex of the oncolites is irregular.

clase phenocrysts in a groundmass with abundant red to brown grains, which are probably altered olivine. Zeolites occur in a few (5%) of the large (up to 2 mm) irregular vesicles. Some of the zeolites are stained red in parts.

The volcanic breccia in Unit II occurs at Intervals 144-879A-19R-1, 18–53 cm, -19R-1, 95–134 cm, and -19R-2, 0–137 cm. The matrix of the breccia is weak red (10R 4/4) to reddish brown (2.5YR 5/3). Clasts within the breccia are usually 1 cm in size, but they can range up to 2–3 cm, and are composed of basalt. Two types of basalt clasts are observed in the breccia. The first type is highly vesicular (30%–40%) and pale yellow (2.5Y 7/4). Vesicles are spherical, 0.03–0.08 mm, and larger, ~1 mm, more irregularly shaped. Most of these vesicles are filled by zeolites. The basalt contains 1% of euhedral plagioclase phenocrysts (up to 1 mm), 2% of euhedral olivine microphenocrysts (<0.03 mm, altered to red brown iddingsite). The groundmass contains abundant plagioclase laths (0.03–0.1 mm) with poorly developed flow alignments. The second type of basalt clast is very dusky red (10R 2.5/2) to dark gray (5YR 4/1), with less than 10% vesicles. Vesicles are spherical to irregularly shaped, large (about 1 mm), and zeolite filled. The zeolites are commonly stained red. These second type of clasts contain 1–2% euhedral plagioclase phenocrysts (up to 0.75 mm) and 1% euhedral olivine (up to 0.25 mm, altered to red to brown iddingsite). The groundmass contains abundant plagioclase laths, some up to 0.25 mm. The margins of smaller clasts commonly are altered to bright red.

The claystone of Unit II is entirely contained in Core 144-879A-20R. It is dark red (10R 3/6), dusky red (10R 3/3), and reddish black (10R 2.5/1) and has a relict volcanic breccia texture. Clasts of dusky red and reddish black are basalt altered to clay, whereas the matrix is dark red clay. Most reddish black clasts are under 2 cm; however, a few are up to 15 cm. The claystone is commonly well lithified and highly fractured; in some places (e.g., Interval 144-879A-20R-5, 35–51 cm), it may be incompletely altered to clay.

The conglomerate of Unit II is matrix supported and dark brown (10YR 3/3) in color; it consists of isolated pebbles in a sandy matrix. Pebble size generally increases with increasing depth. At the top of Section 144-879A-21R-1, the pebbles average 0.5 mm to 1 cm in size, whereas at Section 144-879A-21R-1, 25 cm, pebble size gradually

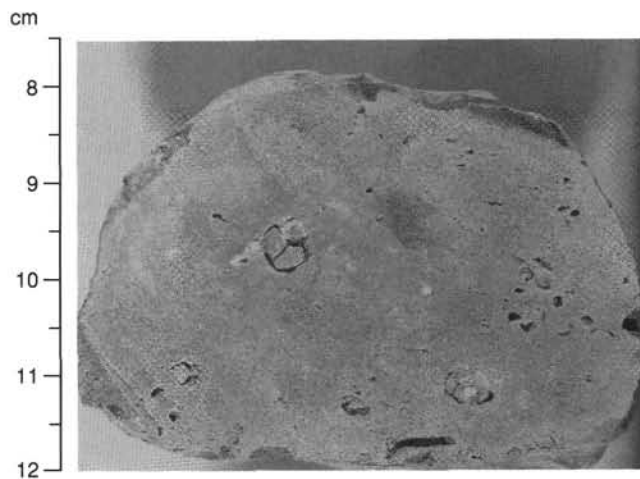


Figure 9. Close-up core photograph of skeletal wackestone characteristic of the lithology of Subunit IB (Interval 144-879A-15R-1, 8–12 cm).

increases to 1.0–1.5 cm. The largest pebble is 4 cm across. Pebbles are composed of orange and yellow brown (10YR 6/6), highly vesicular aphyric basalt. Some of the clasts show multiple color zonation caused by weathering. The matrix of the conglomerate is coarse volcanic sand. The conglomerate is underlain by pale yellowish green volcanic breccia. The contact between these two lithofacies is sharp.

### Unit III

Interval: Sections 144-879A-21R-2, 76 cm to -24R-1, 105 cm  
Depth: 191.0–226.5 mbsf  
Age: indeterminate

Unit III consists of peperite basalt. Refer to “Igneous Petrology” section, this chapter, for a detailed discussion of the basalts that comprise Unit III.

### Preliminary Interpretation of Depositional History

Given the low recovery at Site 879, especially in the platform carbonate sequence (average <5%), a reconstruction of the depositional history is highly speculative. Nevertheless, an overview of the depositional history recovered at Site 879 (Takuyo-Daisan Guyot) can be inferred (Fig. 16). We discuss below our interpretation of the depositional history.

The recovered portion of the volcanic basement is comprised of the peperite basalts of Unit III. Intercalated with this basalt are sand-sized volcanoclastics comprised mainly by vesicular glass and minor basalt fragments. The sand-sized volcanics are locally in sharp subvertical contact with the basalt, suggesting basaltic lava intrusion into wet sediments. Refer to “Igneous Petrology” section (this chapter) for a detailed discussion of the origin of these peperite basalts.

Deposition of Unit II sediments began with a thin veneer of pale yellowish volcanic breccia that is sharply overlain by a dark brown, matrix-supported conglomerate. The conglomerate includes pebbles of highly vesicular aphyric basalt that are weathered orange and yellow brown. This basal conglomerate is itself overlain by dusky red volcanic breccia. This breccia is comprised of basalt clasts, some of which are vesicular, others slightly plagioclase phytic, microcrystalline. The matrix is red clay with sand-sized volcanic debris. Extensive alteration of the breccia, in concert with pervasive coring disturbance, make it difficult to assess the depositional history of these sediments. The intensive reddish color of the breccia is consistent with the oxidation of Unit II in response to subaerial weathering.

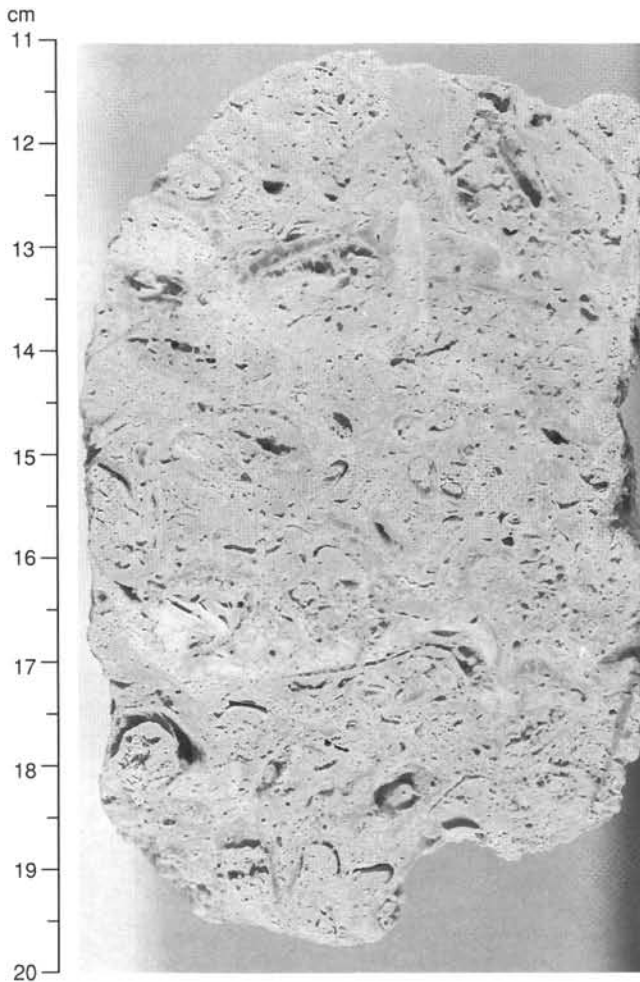


Figure 10. Close-up core photograph of skeletal rudstone with various ornamented bivalves (possibly some rudists) and small gastropods (Interval 144-879A-11R-1, 11–20 cm). This lithology is a minor component of Subunit IB.

Initial flooding of the volcanic edifice at Takuyo-Daisan Guyot by marine waters is reflected in the deposition of mottled calcareous sandstone, gastropod rudstone, argillaceous limestone, and sandstone with volcanic grains that comprise Subunit IE. The basal sandstone includes particles of coal, suggesting that a vegetated paleo-island existed at this site. The top of Subunit IE is a matrix-supported volcanic conglomerate with well-rounded basalt pebbles and molluscan molds in the matrix. Such a combination is consistent with deposition in a shallow-marine environment, possibly in a near-shore environment after river transport.

The argillaceous limestone and sandstone with volcanic grains of Subunit ID were probably deposited in a similar environment as the sediments of Subunit IE. The presence of volcanic grains indicates that a volcanic source, possibly a remnant volcanic island, was still being actively eroded. The occurrence of pelagic microfossils (see “Biostratigraphy” section, this chapter) in this subunit indicates periodic connections with the open-marine environment. Lastly, the presence of pyrite-rich intervals in Subunit ID indicates that reducing conditions occurred sporadically in the shallow-marine environment in which these sediments were deposited.

Sediments of Subunit IC document the diminishing contribution of volcanoclastic sediments and the dominance of shallow-marine carbonate deposition. Limestones of Subunit IC are dominated by skeletal wackestone with subordinate amounts of skeletal packstone. Carbonate components include oncoids, gastropod fragments, abun-

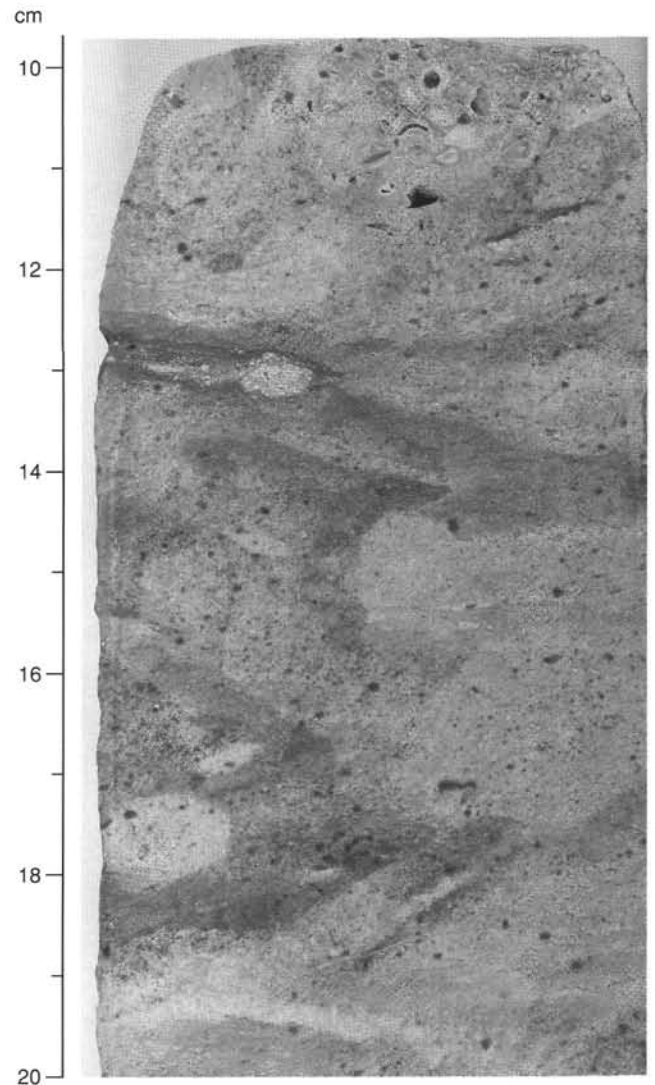


Figure 11. Close-up core photograph of mottled skeletal wackestone with altered basalt grains that occurs in Subunit IC (Interval 144-879A-16R-1, 10–20 cm).

dant bivalve fragments (including rudists), common peloids, common benthic foraminifers (miliolids, textulariids, and *Vercorsella*), and few echinoids. The dominance of wackestone fabric is consistent with low energy conditions, perhaps in an interior portion of the developing carbonate platform at Site 879.

Skeletal packstone and wackestone, with rare grainstone, attests to complete development of a carbonate platform at the time Subunit IB was deposited. The absence of volcanoclastics may be evidence that the weathered volcanic edifice was completely submerged by this time. The dominance of muddy skeletal carbonate and the rare occurrence of mud-free grainstone suggests that these limestones were deposited in an interior, lower energy section of the carbonate platform.

The last record of carbonate deposition at Takuyo-Daisan Guyot is the coral-molluscan rudstone and floatstone of Subunit IA. Components of the rudstone include gastropods (nerineids and cerithids) and bivalve shell fragments (both thin-shelled forms, thick-walled oysters, and probable fragments radiolitid rudists). Components of the floatstone include corals (1–7 cm), bivalves (thin-shelled forms, oysters, and a few probable rudist fragments), cyanobacterial bushes (*Ortonella*), benthic foraminifers (orbitolinids, miliolids), and very rare green algae (dasycladaceans). These biotic associations are consistent with deposition in an open-marine, high-energy section of a

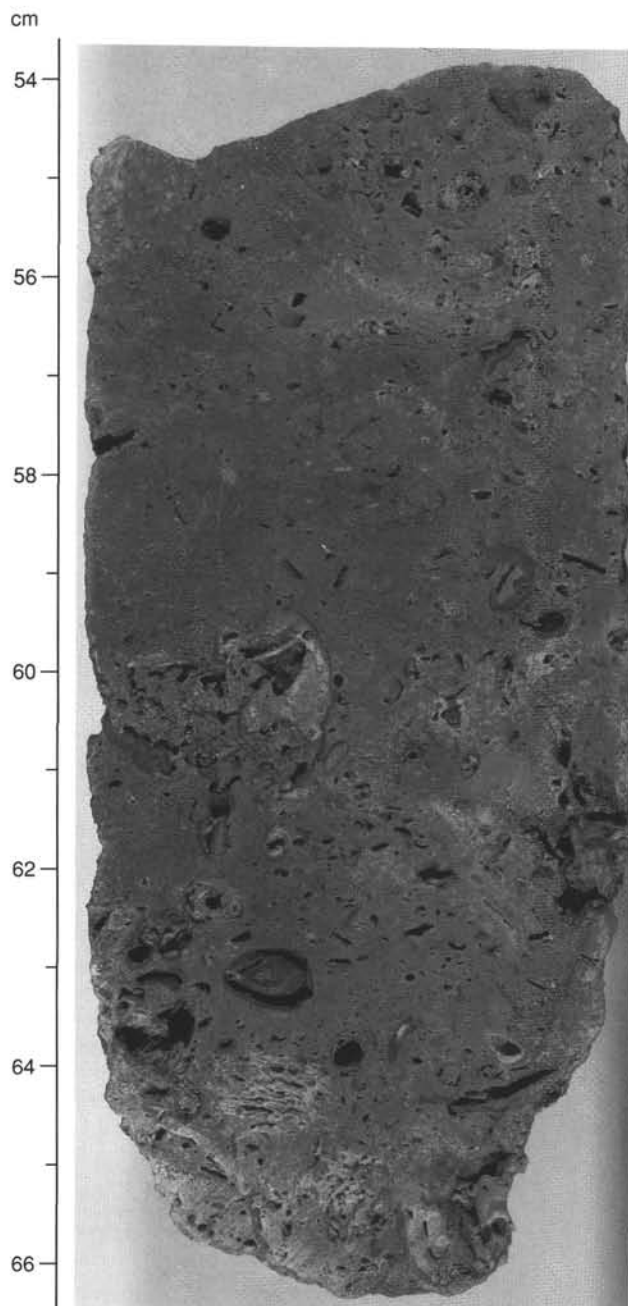


Figure 12. Close-up core photograph of pyrite-rich skeletal packstone in Subunit ID (Interval 144-879A-17R-1, 54–66 cm).

carbonate platform. However, despite the location of Site 879 on the perimeter mound at the edge of Takuyo-Daisan Guyot, no unequivocal evidence of reef development was recovered.

## BIOSTRATIGRAPHY

### Introduction

Hole 879A was drilled on the eastern margin of Takuyo-Daisan Guyot to penetrate a Cretaceous carbonate platform and the underlying basement. The lack of pelagic ooze and the limited time available for shipboard analysis precluded examination for siliceous microplankton. Age assignments are based on the distribution of calcareous microfossils. The available age information is illustrated in Figure 17.

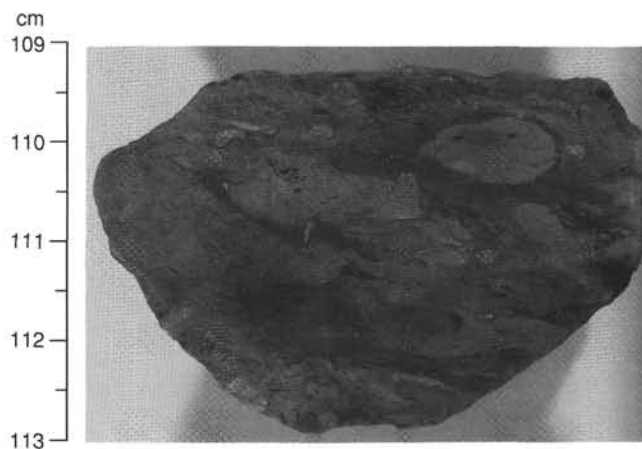


Figure 13. Close-up core photograph of argillaceous limestone with woody material that is the characteristic facies of Subunit ID (Interval 144-879A-17R-1, 109–113 cm).

### Calcareous Nannofossils

Soft chalk on the surface of a phosphatized limestone fragment (Sample 144-879A-5R-1, 0–2 cm) contained common, moderately preserved nannofossils including *Discoaster barbadiensis*, *Discoaster saipanensis*, *Discoaster strictus*, *Reticulofenestra umbilica*, *Reticulofenestra dictyoda*, and *Dictyococcites bisecta*. This assemblage indicates the *R. umbilica* Zone (CP14) of late middle Eocene age. The absence of sphenoliths implies cooler surface waters. This is corroborated by the dominance of reticulofenestrids and the high abundance of *Coccolithus eopelagicus*. However, the chiasmoliths, which would normally be expected in cooler water assemblages, are also absent.

Several samples from Cores 144-879A-17R and -18R contain sparse, moderately preserved nannofossil assemblages. The richest of these (Sample 144-879A-17R-1, 73–74 cm) contains species that include *Eprolithus floralis*, *Nannoconus truittii*, *Rucinolithus terebrodentarius*, *Rucinolithus irregularis*, *Braarudosphaera africana*, and *Rhagodiscus asper*. The relatively high abundance of *N. truittii* probably indicates the *N. truittii* Acme of late Aptian age. This is corroborated by the stratigraphic placement based on benthic foraminifers.

### Planktonic Foraminifers

Rare planktonic foraminifers, in variable states of preservation, were isolated from the saw cuttings of Core 144-879A-1R. *Neogloboquadrina acostaensis*, *N. pachyderma*, and *Globorotalia inflata*, possibly of Holocene age, were identified. A poorly preserved specimen that possibly belongs to the genus *Acarinina* (Paleocene-Eocene) was also found. These are presumably derived from the downhole contamination of pelagic material from the top of the hole.

Planktonic foraminifers were observed on the surface of the split core in Interval 144-879A-16R-1, 10–48 cm. These include specimens of *Hedbergella* and *Globigerinelloides*. Later examination should allow species identifications and possible age assignments.

### Benthic Foraminifers

The distribution of large benthic foraminifers is illustrated in Figure 17. Specimens of *Mesorbitolina* sp. cf. *M. subconca*, *Paracoskinolina* sp. cf. *P. sunnilandensis*, and *Cuneolina* gr. *C. parva-pavonia* in Cores 144-879A-2R through -6R indicate a late Aptian to Albanian age for this interval. The interval from Core 144-879A-11R through -18R contains a significantly different assemblage including species of *Nautilocolina*, *Vercorsella*, and *Hagenowina* sp. A. This assemblage indicates a late Aptian age for this interval.

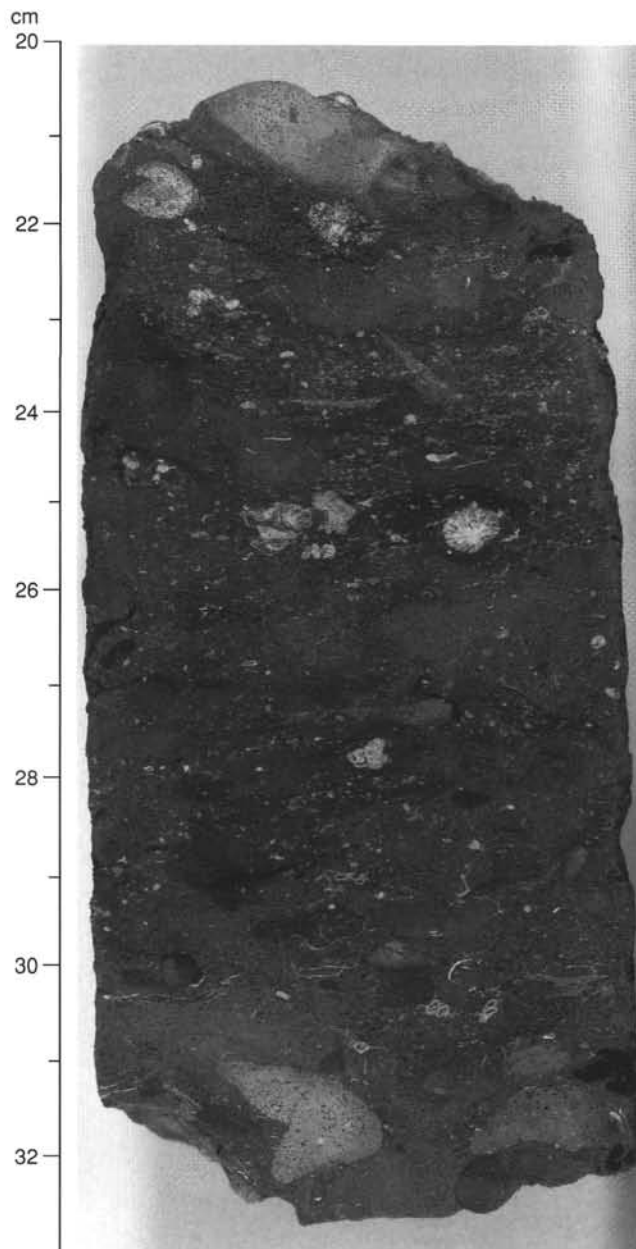


Figure 14. Close-up core photograph of dark gray, pebbly calcareous sandstone that is the characteristic facies of Subunit IE (Interval 144-879A-17R-2, 21–32 cm).

### Palynology

Three organic-rich samples, prepared as smear slides without the use of acid, were investigated for their visual organic characteristics.

Sample 144-879A-17R-2, 24–25 cm, is a dark gray argillaceous limestone that was found to contain common woody material. The brownish yellow color of a single smooth, subtriangular, trilete spore discovered in the smear slide indicates a low-volatile lignite to sub-bituminous level of coalification. This visual estimate broadly agrees with geochemical results that indicate insignificant thermal maturation of this sample (see “Organic Geochemistry” section, this chapter).

Small (>1 mm) black fragments from Sample 144-879A-17R-CC were found to contain a light brown, structureless, resin-like material, fragments of which have a platy, corroded texture. This material is of uncertain affinity.

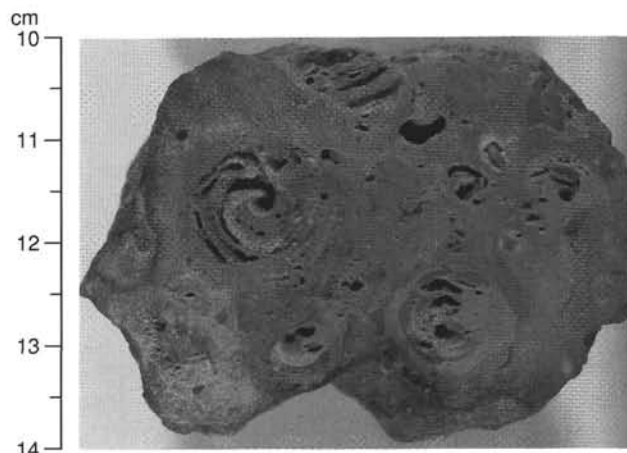


Figure 15. Close-up core photograph of very pale brown (10YR 7/4), extensively bioturbated, gastropod rudstone near the base of Subunit IE (Interval 144-879A-18R-1, 10–14 cm).

Sample 144-879A-19R-2, 0–2 cm, is from a dark brown, coaly lithology. Microscope analysis reveals abundant woody tissues and light brown resinous fragments.

The color of organic material in all the samples examined suggests thermal maturation within the range of low-volatile lignite to sub-bituminous levels of coalification.

### Summary

The presence of rare Neogene to Holocene planktonic foraminifers and late middle Eocene calcareous nannofossils implies the presence of a thin veneer of pelagic calcareous sediment above the platform carbonate sequence at this site. Poor recovery, lack of time, and the unavailability of thin sections hampered age determinations at this site. However, sufficient material was available to establish a late Aptian to Albian age for the platform carbonate sequence. The underlying burrowed and argillaceous limestone sequences contain rare calcareous plankton of late Aptian age. This argillaceous limestone contains common woody material of a low-volatile lignite to sub-bituminous level of coalification.

### PALEOMAGNETISM

Initial magnetic susceptibility was measured at 5-cm intervals on most whole-round cores from Core 144-879A-17R to -24R, after spacers had been placed into the liner to establish the curated positions. The susceptibility in the volcanic basement is generally high ( $>10^{-4}$  cgs; Fig. 18). The susceptibility of the claystone interval (169.7–187.0 mbsf) is nearly 1 order of magnitude higher than that of the peperite basalt at the base of Hole 879A. The high remanent intensity of the latter unit suggests that the low susceptibility may, in part, be related to a finer grain size.

Remanence measurements with the pass-through cryogenic magnetometer were made on the archive halves of the limestone of Cores 144-879A-16R and -17R. No magnetostratigraphic interpretation of the data was possible, but the inclinations are mostly shallow and negative. Further shore-based work will address whether these limestone samples preserve an original magnetization.

Three discrete samples from the volcanic basement (two basalt samples and one from the interstitial volcanoclastic material) were demagnetized and measured with the pass-through cryogenic magnetometer. They have nearly univectorial magnetization and a characteristic direction that is well defined by alternating-field (AF) demagnetization (Fig. 19). The natural remanent magnetization (NRM) in-

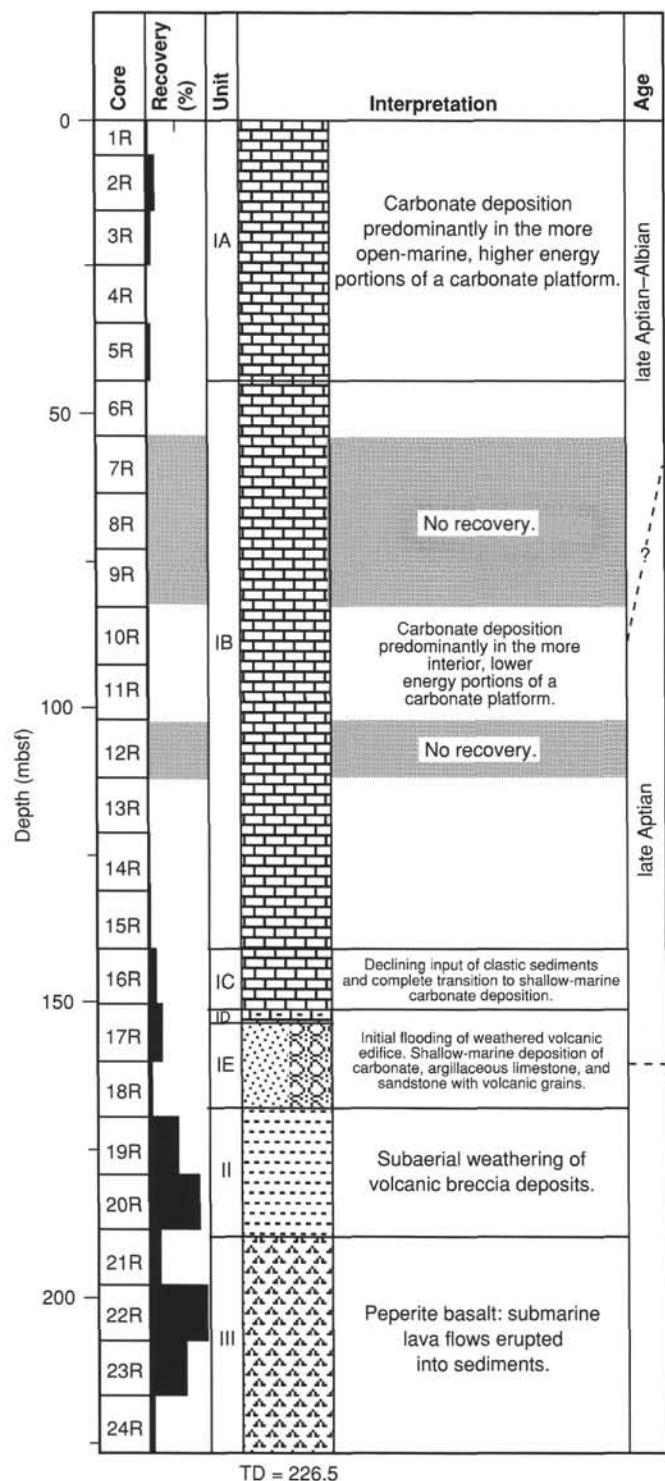


Figure 16. Summary of preliminary interpretations of depositional history at Site 879.

tensity of the two basalt samples are 5 and 11  $\text{Am}^{-1}$ ; the NRM intensity of the volcanoclastic material is 1 order of magnitude lower ( $0.1 \text{ Am}^{-1}$ ). The inclinations of the characteristic remanent magnetization are negative (Table 4).

Remanence measurements also included whole-core measurements of the claystone interval and volcanic basement from the archive halves (Fig. 20). With few exceptions (e.g., near 170 mbsf), the inclination is generally negative. Most of the positive inclinations are demonstrably

related to the presence of large basaltic clasts, which presumably retain their original magnetization. The inclination of the whole-core data (about  $-15^\circ$ ) is similar to that derived from discrete sample measurements ( $-18^\circ$ ). In view of the late Aptian age of the overlying sediments ("Biostratigraphy" section, this chapter), the simplest interpretation of this data is that they represent a normal polarity magnetization acquired at a paleolatitude of approximately  $9^\circ\text{S}$ . However, the logging results indicate that Hole 879A dips  $10^\circ$  toward  $300^\circ$ . The effect of the deviation from vertical on the remanent inclinations depends strongly on the remanent declination. Declinations within  $20^\circ$  of north yield corrected inclinations of  $10^\circ$  (declination  $340^\circ$ ) to  $-16^\circ$  (declination  $020^\circ$ ), corresponding to slightly lower paleolatitudes.

## INORGANIC GEOCHEMISTRY

### Interstitial Waters

Interstitial waters were squeezed from two core samples in Hole 879A. Both of these samples came from clays associated with basalts. These samples were processed according to the methods outlined in the "Explanatory Notes" chapter (this volume); however, time limitations restricted shipboard analyses to the measurement of pH, alkalinity, and salinity in Sample 144-879A-20R-4, 140–150 cm. These data are presented in Table 5.

## ORGANIC GEOCHEMISTRY

### Introduction

Site 879 was drilled on the marginal rim of Takuyo-Daisan Guyot. The type of rocks encountered at the site were (from top to bottom): platform carbonate with argillaceous sandy limestone and volcanic conglomerate at the bottom (Lithologic Unit I; see "Lithostratigraphy" section, this chapter); clay, claystone, and volcanic breccia (Unit II); and basalt (Unit III).

The analytical program for Hole 879A included chemical analysis and pyrolysis. Twenty-five samples from the platform carbonate and the underlying argillaceous limestone were analyzed for inorganic carbon (IC). Of these, fourteen samples were selected for total organic carbon (TOC), nitrogen (N), and total sulfur (TS) analyses. One sample from the argillaceous limestone was analyzed for organic matter type by pyrolysis. The procedures used for the analytical program are described in the "Organic Geochemistry" section, "Explanatory Notes" chapter (this volume).

### Volatile Hydrocarbons

The shipboard safety and pollution monitoring program requires measurements of light hydrocarbon gases ( $\text{C}_1$  to  $\text{C}_3$ ) in cores immediately after retrieval onto the core deck. However, hydrocarbon gases were not considered a safety hazard at this site, and no sampling for headspace gas was attempted.

### Carbonate Carbon

Inorganic carbon (IC) content was measured in 25 samples from Hole 879A with the Coulometrics carbon dioxide coulometer and reported as weight% calcium carbonate. Sampling was performed in a way to obtain representative material with regard to both lithotypes and depth. Sixteen microsamples from the limestone (approximately 100 mg each) were collected by hand drilling using a standard 5-mm drill bit. Moreover, five samples from the muddy intervals were taken directly from the cutting surface. Two samples from the clay interlayering the basalt breccia were collected from the squeeze-cake left after interstitial water sampling. No sampling was done in the basalt. Results of the inorganic carbon analyses are given in Table 6. Calcium carbonate data are shown in Figure 21.

The platform carbonate from Lithologic Unit I had carbonate contents from 80% to 100% (average  $\text{CaCO}_3$  for Subunits IA to IC =

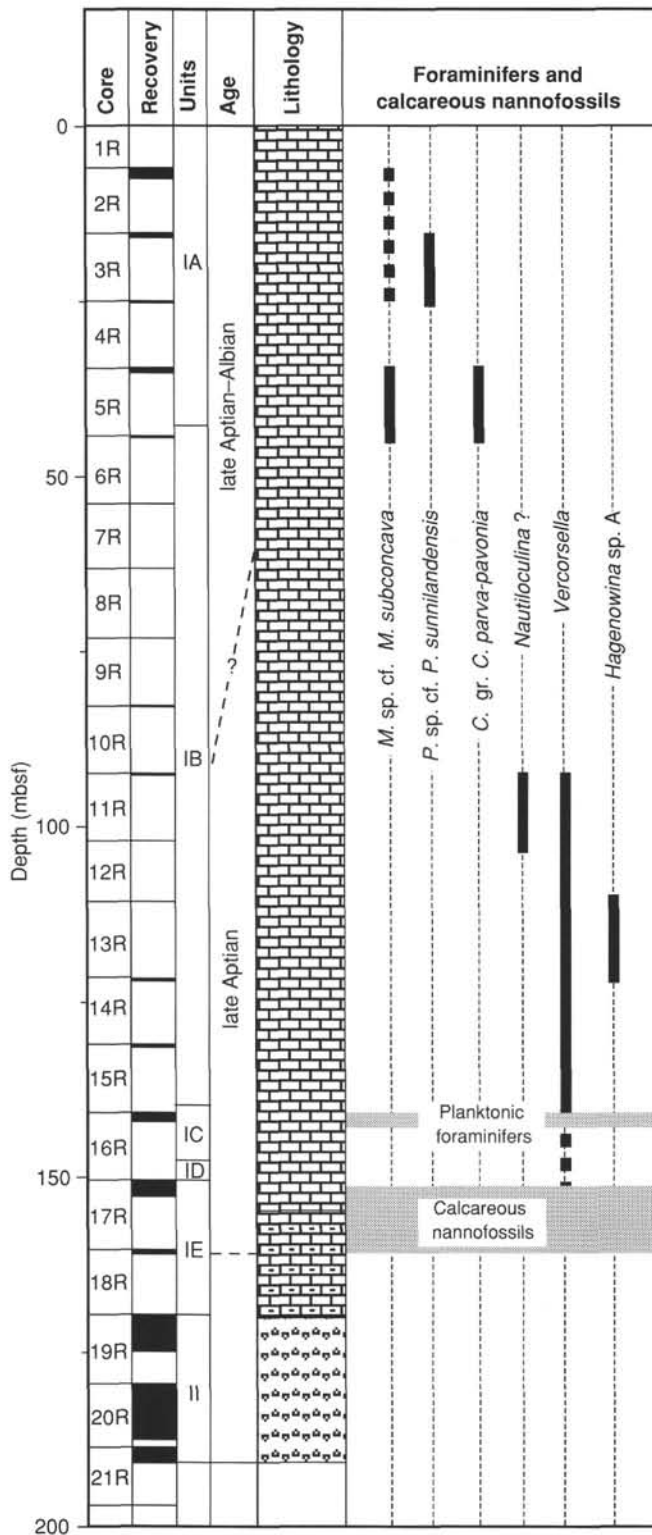


Figure 17. Distribution of in-situ foraminifers and calcareous nannofossils in the sedimentary sequence of Hole 879A.

93.5%). The lowest values were found in the deeper part of the platform. The argillaceous, sandy limestone of Subunit ID had varying, but low carbonate values (average  $\text{CaCO}_3 = 33\%$ ). This subunit included two mudstone beds, which were virtually carbonate-free (Samples 144-879A-17R-2, 58–63 cm, and 144-879A-17R-2, 71–72 cm), and marked the bottom of two cycles of upward-increasing carbonate content (Fig. 21). The highest carbonate content in these cycles coincided with the most intensive bioturbation. A similar, but less pronounced, cycle was observed in Subunit IE at 161 m, where gray-greenish, carbonate-free clay was overlain by bioturbated calcareous sand and rudstone (Samples 144-879A-18R-1, 43–44 cm, -18R-1, 33–34 cm, and -18R-1, 4–5 cm). The brown clay beds of Lithologic Unit II contained no carbonate.

### Organic Carbon and Total Sulfur

The content of total carbon (TC), nitrogen (N), and total sulfur (TS) was determined using the Carlo Erba Model NA1500 elemental analyzer. Total organic carbon (TOC) values were calculated from the difference between TC and IC. Detection limits for TOC, N, and TS are 0.2%, 0.02%, and 0.02% respectively. Analyses were performed on 13 of the samples used for carbonate carbon determinations. The results of the TOC, N, and TS analyses are given in Table 6 and Figures 22–23.

In the platform carbonate of Lithologic Unit I, organic carbon and sulfur contents were determined only in the gray, skeletal wackestone of Subunit IC. The samples were found to contain less than 0.2% organic carbon and 0.8% sulfur. The gray coloring is probably caused by the increased clay content rather than by changes in the organic carbon or pyrite contents.

The argillaceous limestone in Lithologic Unit ID (the term is actually misleading; the rocks are dominantly calcareous sandstone and mudstone) showed the highest organic carbon and sulfur contents encountered at Site 879 (Fig. 22). The highest TOC values were seen in the carbonate-poor mudstone levels forming the bases of the two cycles mentioned above. These levels also coincided with increased TS values. However, only the upper mudstone was significantly enriched in sulfur (highest TS = 3.7%). At this level, pyrite was abundant, mainly observed as aggregates of fine-grained, framboidal crystals. The TS/TOC ratios between 2 and 5 indicate significant sulfur reduction and migration of sulfide-rich solutions (Fig. 23). Several flattened, centimeter-wide pieces of wood were observed in the mudstone. The boundary between the TOC-rich and TS-rich mudstone and the overlying gray, muddy limestone (which does not coincide with the boundary between Subunits IC and ID) was marked by a loose fragment of wood ( $3 \times 2 \times 0.5$  cm) and probably represented a considerable lack of core recovery. Thus, the upward termination of the sulfur-reducing episode could not be evaluated here. Nitrogen content was low (<0.3%) in all samples.

### Organic Matter Type and Thermal Maturation Level

Shipboard geochemical characterization of organic matter is normally performed by Rock-Eval (RE) and pyrolysis gas chromatographic (Py-GC) analysis. Only samples containing more than 1% organic matter are considered suitable for these types of analyses. During the time spent at Site 879, the Rock-Eval instrument was out of order, and organic matter characterization was confined to the Geofina instrument.

Two samples from Hole 879A were analyzed by pyrolysis. One was from a calcareous, sandy mudstone from Subunit ID rich in thin-walled shell fragments probably of molluscan origin (Sample 144-879A-17R-2, 24–25 cm). The other was from a 5-cm-thick lignite bed encountered at top of the weathered, volcanic breccia in

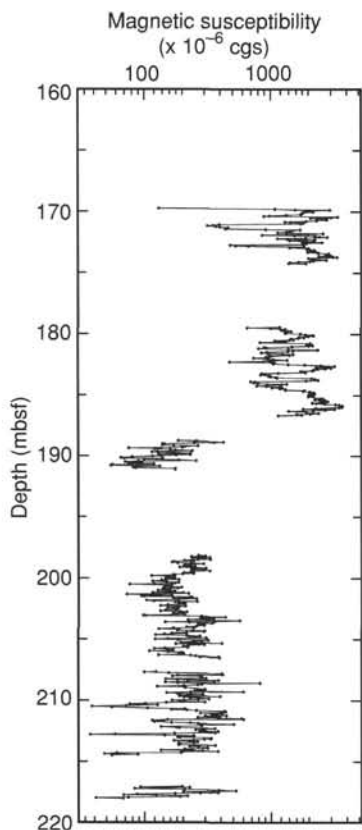


Figure 18. Magnetic susceptibility variations at Site 879.

Unit II (Sample 144-879A-19R-1, 0–5 cm). Both samples were also evaluated visually by palynologic methods (see “Biostratigraphy” section, this volume).

The sample from the calcareous mudstone was low in volatiles and produced very little hydrocarbon upon pyrolysis (hydrogen index [HI] = 46). Moreover, thermal maturity was very low ( $T_{\max} = 397^{\circ}\text{C}$ ). The organic matter belonged to a type III (woody or vitrinitic) kerogen. These observations are in accordance with the visual classification of the organic matter as being mainly of woody origin (“Biostratigraphy” section, this volume). The organic matter was of a light brown color corresponding to thermally immature conditions.

The lignite sample was not analyzed for organic carbon before pyrolysis, which excluded determination of the hydrogen index. The  $T_{\max}$  value of  $371^{\circ}\text{C}$  was abnormally low and did not reflect actual thermal maturation. Visual inspection of the sample suggested that the lignite was partly resinous and of low thermal maturity (“Biostratigraphy” section, this volume).

### Interpretation of Organic Facies and Depositional Environments

Three major depositional environments were represented at the site: (1) shallow-water marine, dominated by platform carbonate; (2) shallow-water transitional, dominated by intercalating platform limestone, argillaceous limestone, and mudstone; and (3) terrestrial, dominated by variegated clay and weathered basalt. The preservation potential for organic matter was very low in the first environment, indicating deposition under oxic conditions. A change in depositional environment to more restricted conditions toward the bottom of the carbonate platform was suggested by the slightly increased TOC and TS values seen in Subunit IC.

Sample 144-879A-22R-2, 91 cm

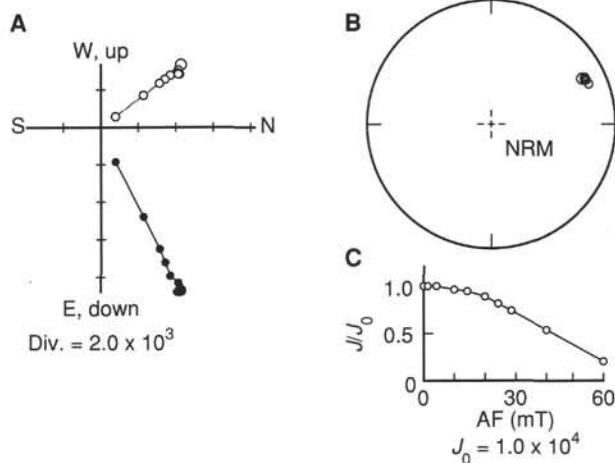


Figure 19. Alternating-field (AF) demagnetization results for Sample 144-879A-22R-2, 91 cm, from volcanic basement. Demagnetization fields are 0, 2.5, 5, 10, 15, 20, 29, 40, and 60 mT. **A.** Orthogonal vector plot of progressive AF demagnetization. Closed circles represent horizontal components of the magnetization, and open circles represent vertical components. **B.** Stereonet plot of vector end-points after progressive demagnetization. **C.** Variation of intensity after progressive AF demagnetization.

**Table 4. Results of demagnetization of samples from volcanic basement, Hole 879A.**

| Core, section, interval (cm) | Lithology      | Inclination (degrees) |
|------------------------------|----------------|-----------------------|
| 144-879A-22R-1, 73–75        | Volcaniclastic | –5.8                  |
| 22R-2, 91–93                 | Basalt         | –17.6                 |
| 22R-5, 44–46                 | Basalt         | –18.0                 |

The shallow-water transitional environment in Subunit ID was characterized by rapid changes between oxic conditions dominated by platform-type carbonates low in organic matter and anoxic conditions dominated by mudstone and argillaceous limestone rich in terrigenous organic matter. The mudstone probably represented periods of increased terrestrial flux into an otherwise well-established carbonate-producing environment. Two such events of increased terrestrial flux could be identified in Subunit ID. Only after the last event did bacterial sulfate-reducing conditions remain long enough for substantial amounts of pyrite to form.

The terrestrial environment generally had a low potential for preservation of organic matter. However, the identification of a lignite bed at the top of the weathered basalt did indicate local subaqueous environments where minor amounts of plant material could settle under anoxic conditions. The occurrence of pyrite at the top of the lignite bed pointed to some marine influence.

### Conclusions

The following conclusions can be made regarding the organic geochemistry at Site 879:

1. The platform carbonate of Lithologic Unit I contained only insignificant amounts of organic matter and sulfur.
2. The gray color of the skeletal wackestone in Subunit IC was caused by increased clay content rather than by organic matter or pyrite.
3. Two cycles consisting of organic-rich mud changing upward into organic-poor platform carbonates were identified in Subunit ID.

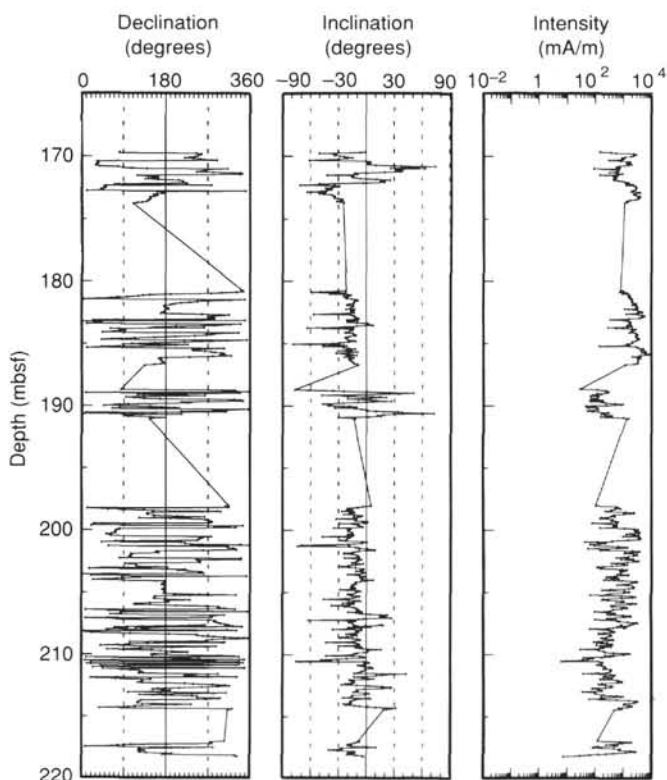


Figure 20. Declination, inclination, and intensity variations for Cores 144-879A-19R to -24R after demagnetization at 15 mT with the pass-through cryogenic magnetometer.

The organic matter was dominated by terrestrial plant material, suggesting a terrigenous origin for the muds.

4. A sulfur enrichment was found in the upper of the two mud-rich intervals. The enrichment was interpreted as a result of bacterial sulfate reduction of organic matter in an anoxic, seawater dominated environment.

5. Thermal alteration of organic matter was low, corresponding to immature conditions with regard to hydrocarbon formation ( $T_{\max} = 397^{\circ}\text{C}$ ). The level of thermal maturity could be explained from influence of burial alone.

## IGNEOUS PETROLOGY

Site 879 was drilled on a perimeter ridge near the southern edge of Takuyo-Daisan Guyot. At 264.9 mbsf, Hole 879A passed from the pebble conglomerate of Lithologic Unit II into a complex, intercalated mixture of basalt and volcanic breccia. We interpret this mixture as a peperite, formed by intrusion of basaltic lava into soft, wet volcanic breccia. Approximately 19.5 m of peperite was recovered and the hole ended at 299.3 mbsf (Table 7).

Basaltic lava forms irregularly shaped, subspherical, pillow-like bodies, ranging in size from less than a centimeter to a meter or more. Narrow relict-chilled margins are present along many of the pillow surfaces. The basalt is quite uniform in texture throughout the recovered interval. It is highly plagioclase-phyric with approximately 20% plagioclase and minor olivine phenocrysts in a microcrystalline groundmass. Plagioclase occurs as subhedral, rather elongate prisms ranging in length from about 0.5 to 8.0 mm. In the fresher parts of the basalt, these phenocrysts are transparent and remarkably fresh; for the most part, however, they appear partially altered to white clay or zeolite and are often stained red or green. Many of the larger prisms can be seen to contain dark-colored inclusions, most likely melt

Table 5. Surface seawater and interstitial water geochemical data, Hole 879A.

| Core, section, interval (cm) | Depth (mbsf) | pH   | Alkalinity (mM) | Salinity (g/kg) |
|------------------------------|--------------|------|-----------------|-----------------|
| Surface seawater             | 0            | 8.07 | 2.375           | 35              |
| 144-879A-17R-2, 58-63        |              | —    | —               | —               |
| 20R-4, 140-150               |              | 7.61 | 2.509           | 34              |

inclusions, in their centers. Sparse (1%), euhedral, diamond-shaped olivine microphenocrysts occur throughout the basalt. They have been completely altered to reddish brown iddingsite. The matrix of the basalt is microcrystalline. Its color is medium gray where fresh material has been preserved in pillow centers, away from veins. Through most of the section, however, the matrix has a slight reddish discoloration reflecting pervasive alteration, and distinct, iron-stained alteration fronts occur in the vicinity of veins. Approaching many of the pillow margins, subtle variations in color and texture reflect the presence of narrow (a few millimeters), chilled margins. The margins themselves are marked by a narrow (1–2 mm) band of reddish brown, altered glass.

The irregularly shaped spaces between the basalt pillows are occupied by grayish green volcanic breccia (Fig. 24). The components of the breccia have been completely replaced by soft clay and/or zeolite minerals, but primary textural features are retained in great detail. About 60% of the original clasts are fragile, angular, highly vesicular, glassy basalt. The remaining clasts are also angular and include a variety of nonvesicular basalts. Very little of the interpillow material has been formed by fragmentation of the associated plagioclase-phyric lava, although numerous, rounded “mini-pillows” are common. Angular fragments of the intrusive basalt do occur, but they are restricted to areas of auto-brecciation, where localized fracturing of pillow margins and invasion of the resulting fractures by sediment has occurred. The matrix of the breccia consists of sand-sized shards of the same glassy vesicular basalt as the larger clasts, cemented by grayish green clay or zeolite. In Interval 144-879A-22R-4, 42–65 cm, well-sorted coarse volcanic sandstone fills the interpillow spaces. This sandstone contains angular, coarse sand-sized (<1 mm) fragments of the same volcanic materials as are found in the breccia. It presumably represents a thin, reworked deposit within the original breccia deposit.

This breccia is very similar in texture and in mode of origin to the polymictic breccias of Hole 878A, although it lacks the included limestone clasts. The dominant vesicular clasts are “juvenile” clasts formed from new magma during eruption, and the remainder are “accidental” clasts formed by explosive fragmentation of preexisting basalt during eruption. The materials in the breccia are derived from a phreatomagmatic volcanic eruption, which predates and is separate from the intrusion of the plagioclase-phyric basalt. The time period between these two volcanic events is not constrained, but it is likely to have been relatively short, perhaps less than a million years, as the intruded sediments were necessarily water saturated with a low bulk density. None of the observed features of either the plagioclase-phyric basalts or the glassy basalt clasts in the breccia provide any indication of the petrologic affinities of these lavas, and no chemical or thin section data are available. The eruptions sampled at this site clearly occurred late in the history of the volcano, but it is not apparent whether they represent a shield-building phase or a later rejuvenated phase of volcanism.

## PHYSICAL PROPERTIES

### Introduction

The objectives of the physical properties measurement program at Site 879 (Takuyo-Daisan Guyot) Hole 879A were (1) to measure standard shipboard physical properties and (2) to differentiate the

**Table 6. Results of geochemical analyses, Hole 879A.**

| Core, section, interval (cm) | Lithology              | Depth (mbsf) | IC (wt%) | CaCO <sub>3</sub> (wt%) | TC (wt%) | TOC (wt%) | N (wt%) | TS (wt%) |
|------------------------------|------------------------|--------------|----------|-------------------------|----------|-----------|---------|----------|
| 144-879A-                    |                        |              |          |                         |          |           |         |          |
| 1R-1, 0-5                    | Limestone              | 0            | 11.74    | 97.80                   |          |           |         |          |
| 2R-1, 32-40                  | Limestone              | 6.42         | 11.84    | 98.60                   |          |           |         |          |
| 3R-1, 29-34                  | Limestone              | 15.79        | 11.76    | 98.00                   |          |           |         |          |
| 5R-1, 37-41                  | Limestone              | 34.97        | 11.84    | 98.60                   |          |           |         |          |
| 10R-1, 15-19                 | Limestone              | 83.05        | 11.68    | 97.30                   |          |           |         |          |
| 11R-1, 23-29                 | Limestone              | 92.73        | 9.64     | 80.30                   |          |           |         |          |
| 14R-1, 13-18                 | Limestone              | 121.63       | 11.54    | 96.10                   |          |           |         |          |
| 16R-1, 40-41                 | Limestone              | 141.20       | 10.79    | 89.90                   | 10.92    | 0.13      | 0.01    | 0        |
| 16R-1, 113-114               | Limestone              | 141.93       | 10.20    | 85.00                   | 10.41    | 0.21      | 0       | 0.83     |
| 17R-1, 28-29                 | Argillaceous limestone | 150.68       | 8.98     | 74.80                   | 9.36     | 0.38      | 0.01    | 0.77     |
| 17R-1, 74-75                 | Mudstone               | 151.14       | 2.10     | 17.50                   | 4.00     | 1.90      | 0.03    | 3.71     |
| 17R-1, 91-95                 | Mudstone               | 151.31       | 0.66     | 5.50                    | 1.53     | 0.87      | 0.02    | 2.07     |
| 17R-1, 109-110               | Limestone              | 151.49       | 9.42     | 78.50                   | 9.63     | 0.21      | 0.01    | 1.21     |
| 17R-1, 124-125               | Argillaceous limestone | 151.64       | 4.85     | 40.40                   | 5.13     | 0.28      | 0       | 0        |
| 17R-2, 24-25                 | Mudstone               | 152.14       | 1.88     | 15.70                   | 3.55     | 1.67      | 0.02    | 0.65     |
| 17R-2, 48-49                 | Argillaceous limestone | 152.38       | 7.60     | 63.30                   | 7.71     | 0.11      | 0       | 0.03     |
| 17R-2, 58-63                 | Mudstone               | 152.48       | 0.14     | 1.20                    |          |           |         |          |
| 17R-2, 71-72                 | Mudstone               | 152.61       | 0.48     | 4.00                    | 0.48     | 0         | 0       | 0        |
| 17R-2, 92-93                 | Limestone              | 152.82       | 11.78    | 98.10                   |          |           |         |          |
| 18R-1, 4-5                   | Limestone              | 160.14       | 11.33    | 94.40                   | 11.55    | 0.22      | 0       | 0        |
| 18R-1, 33-34                 | Limestone              | 160.43       | 10.57    | 88.00                   | 10.82    | 0.25      | 0.01    | 0        |
| 18R-1, 43-44                 | Argillaceous limestone | 160.53       | 8.45     | 70.40                   | 8.65     | 0.20      | 0.01    | 0.23     |
| 19R-1, 0-2                   | Red clay               | 169.70       | 0.05     | 0.40                    |          |           |         |          |
| 20R-4, 140-150               | Red clay               | 185.14       | 0.07     | 0.60                    |          |           |         |          |

Notes: IC = inorganic carbon, CaCO<sub>3</sub> = carbonate carbon calculated as calcium carbonate, TC: total carbon, TOC = total organic carbon, N = nitrogen, TS = total sulfur, and blanks = no determination.

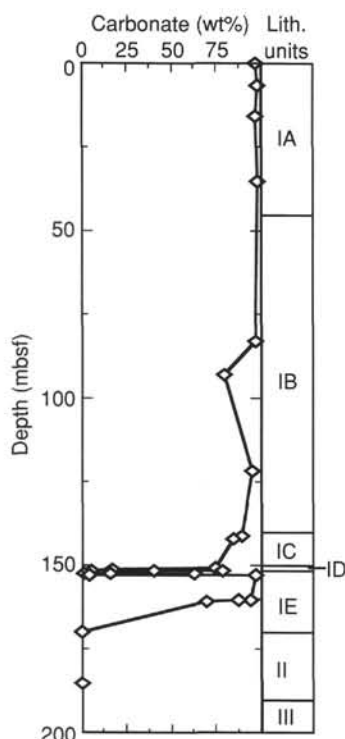


Figure 21. Carbonate content of sediments in Hole 879A, calculated as calcium carbonate. Also shown are the major lithologic units, as given in the "Lithostratigraphy" section (this chapter).

downhole lithology by means of the physical properties. Standard index properties measurements and Hamilton Frame compressional wave velocities, measured using pieces with parallel faces of hard rocks, comprised the major part of the shipboard analyses ("Explanatory Notes" chapter, this volume) at Hole 879A.

Nondestructive measurements of magnetic susceptibility were made of the claystone, conglomerate, and basalt, using sensors mounted on

the multisensor track (MST) after splitting the cores to adjust the curated length to the susceptibility measurements (see "Paleomagnetism" section, this chapter). Coring in Hole 879A was conducted using the RCB from 0 to 226 mbsf.

Sediments recovered at Hole 879A are of late Aptian to Albian age and consist of coral-molluscan rudstone and floatstone with skeletal grainstone (0-44 mbsf), packstone, and wackestone (44-150 mbsf). Argillaceous limestone, calcareous sandstone, claystone, and conglomerate were recovered between 150 and 190 mbsf. Below 190 mbsf, a succession of peperite basalt is weathered to various degrees. Recovery was poor between 0 and 140 mbsf. There was no recovery from Cores 144-879A-7R, -8R, -9R, and -12R.

### Index Properties and Sonic Velocity

Index property profiles vs. depth are shown in Figure 25, and the data are given in Table 8. Wet- and dry-bulk density are seen to have a moderate variation with depth between 0 and 140 mbsf (i.e., Lithologic Subunits IA and IB); however, measurements in the uppermost 120 m are few in number because of the poor recovery. Wet- and dry-bulk density in Subunits IA and IB range from 2.45 to 2.80 g/cm<sup>3</sup> and 2.20 to 2.70 g/cm<sup>3</sup>, respectively. Subunits IC, ID, and IE have lower mean densities and higher mean porosities overall than Subunits IA and IB. Index properties of the claystone/breccia/conglomerate (Lithologic Subunit II) are variable on account of their heterogeneity. However, mean values correspond well with those from other clay/claystone lithologies from Holes 871C, 873A, 874B, and 877A. The clays, as encountered in other holes, have particularly high grain densities, ranging from 3.10 to 3.35 g/cm<sup>3</sup> with a mean of 3.22 g/cm<sup>3</sup>. A single basalt specimen yielded wet- and dry-bulk densities of 2.39 and 2.09 g/cm<sup>3</sup>, respectively, and a grain density of 2.98 g/cm<sup>3</sup>.

Compressional wave velocities range from 3.30 to 5.10 km/s in the upper limestones (Fig. 26 and Table 9), with a mean of 4.51 km/s. In the limestones, sandstones, and conglomerates of Lithologic Subunits IC, ID, and IE velocity is highly variable, ranging from 1.80 to 4.70 km/s, with a mean of 3.00 km/s. The determination of velocity in the underlying claystones proved impossible owing to disaggregation on soaking in distilled water as well as problems in preparing flat and parallel faces on the test specimens. No basalts were taken for velocity testing.

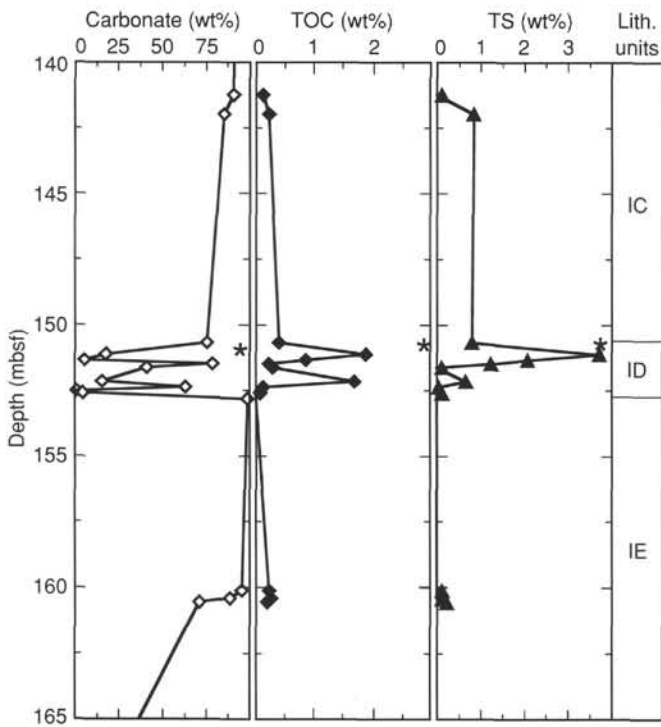


Figure 22. Carbonate (calculated as calcium carbonate), total organic carbon (TOC), and total sulfur (TS) content of sediments from the transition between terrestrial and marine environments in Hole 879A. Lithologic units as in Figure 21. An asterisk marks the occurrence of a loose wood piece in the core.

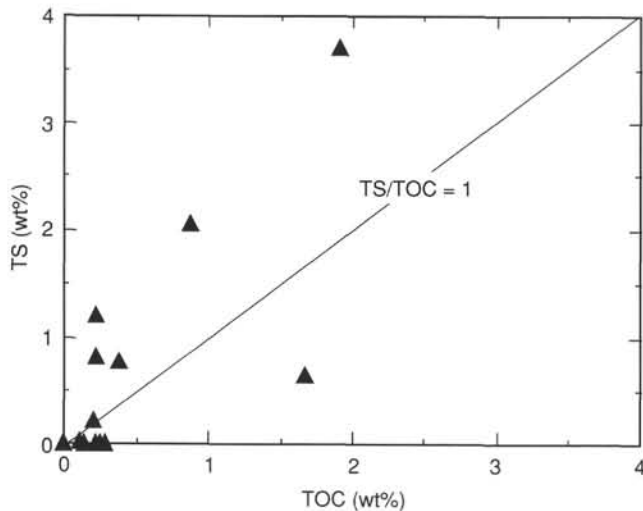


Figure 23. Total sulfur vs. total organic carbon (TS/TOC) in Hole 879A. The distribution represents sulfate-reducing conditions.

**DOWNHOLE MEASUREMENTS AND SEISMIC STRATIGRAPHY**

**Log Types, Processing, and Reliability**

The complete carbonate platform and igneous complex in Hole 879A at the southern rim of Takuyo-Daisan Guyot were logged once with the geophysical and twice with the Formation MicroScanner (FMS) tool strings. The second FMS pass obtained better quality microresistivity imagery of the borehole than the first pass. No geo-

chemical logs were run because of time constraints. Logging measurements were obtained from approximately 210 mbsf, corresponding to the upper part of Core 144-879A-23R, or about 17 m above the base of the hole, to the base of the drill pipe at 40.5 mbsf, corresponding to the lower part of Core 144-879A-5R. Natural gamma-ray radiation measurements were performed up to the sediment surface through the drill pipe. The spacing of tools on the various logging tool strings implies that the lower boundary of logging data from each tool varies (see diagram of tool strings in the "Explanatory Notes" chapter, this volume). These logs are valuable for interpreting the sedimentary succession and for identifying possible discontinuities within the carbonate platform sequence, because core recovery within these 170 m averaged only 5.2% and was less than 3.5% in the upper 150 m. In particular, the FMS provides high-resolution resistivity imagery of the borehole wall within the carbonate platform succession, enabling one to interpret the distribution of the recovered facies.

Logging depths were calibrated to cored intervals by using the known position of the end of the drill pipe during logging (1553.0 m below rig floor [mbrf] or 40.5 mbsf) as detected by the resistivity measurements. This level was at a logging depth of approximately 1552.0 mbrf during all logging runs, implying that 1 m should be added to logging depths to convert to drilled depths. A sharp peak in natural gamma-ray radiation at 1659.3 m corrected below rig floor (146.8 mbsf) indicates that there is no measurable offset between the main geophysics run and the first FMS run. This peak in gamma ray is obscured in the second FMS run, but secondary peaks between 1665 and 1675 mbrf indicate that the depths of the second pass are approximately 0.3 m higher than those in the first pass. The range in daily tide during the drilling and logging operations was less than 1 m in this region (Hydrographer of the Navy, 1991), so we did not compute differential tide corrections to the intercalibration of logging and drilling depths. These depth conversions should place features observed in the logs to within a few tens of centimeters of corresponding features in the cored intervals.

The caliper log of the borehole diameter indicates that most of the borehole above 140 mbsf is widened to 45 cm (18 in.) or greater. This "washed out" interval incorporates the main platform carbonate sequence (Lithologic Subunit IB). Within this zone, the FMS pads are commonly no longer in complete contact with the borehole walls, and one or more of the four traces may be incoherent (see "Explanatory Notes" chapter, this volume). However, there is an average 10° dip of the borehole toward 300° (west-northwest), enabling contact of at least two of the FMS pads through most of this "washout" interval. The lithodensity tool has incomplete contact against the borehole wall, where the borehole diameter exceeds 45 cm (18 in.), resulting in unreliably low values.

**General Log-facies Comparison**

Lithologic units and subunits defined on the basis of the limited core recovery are generally recognized in the composite logs, but some major features observed in the logging measurements were apparently poorly recognized or not recovered during coring. For example, Lithologic Subunits ID and IE, made up of clayey limestone, volcanic conglomerate, and calcareous sandstone, appear to consist of four main pulses of volcanic and clay influx over about a 15-m interval; therefore, the apparent division into two subunits (see "Lithostratigraphy" section, this chapter) is largely an artifact of incomplete recovery.

Fluctuations among bulk density, resistivity, drilling rate, and sonic velocity measurements were observed to correspond within the carbonate platform facies. The limited core recovery indicates that these common fluctuations are controlled mainly by the abundance of lime mud and the degree of cementation (see discussion in "Downhole Measurements and Seismic Stratigraphy" section, "Site 871" chapter, this volume), rather than by mineralogical changes. However, another important control is the size of the widened borehole, especially

**Table 7. Summary of igneous units, Hole 879A.**

| Subunit | Interval  | Description                                       |
|---------|---|---|
| IA      | Sections 144-879A-21R-1, 65 cm, to -24R-1, 106 cm | Fine (3–10 mm) volcanic breccia.                  |
| IB      | Sections 144-879A-21R-1, 65 cm, to -24R-1, 106 cm | Plagioclase basalt (intruded into Subunit IA).    |
| IC      | Interval 144-879A-22R-4, 42–65 cm                 | Volcanic sandstone (finer portion of Subunit IA). |

Notes: Note that Subunit IB is intrusive into Subunit IA and that the two units overlap over the entire basement interval.

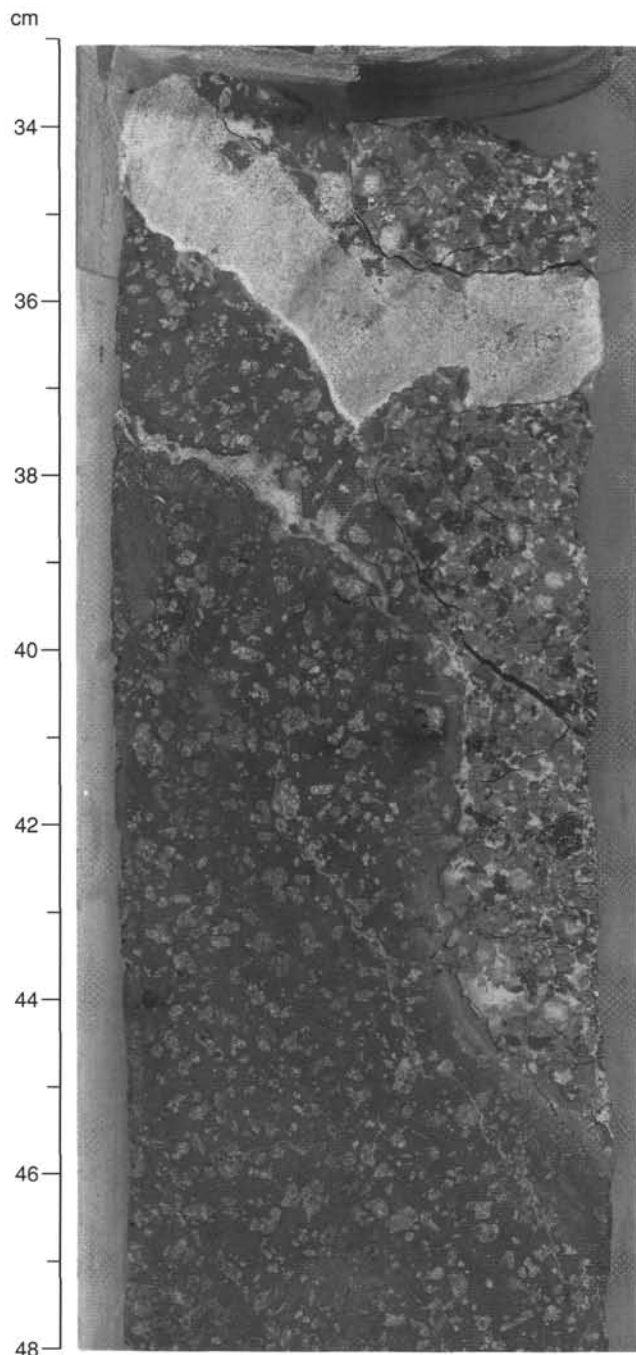


Figure 24. Contact between a basalt pillow and the volcanic breccia into which it has intruded (Interval 144-879A-22R-2, 33–48 cm). The contact runs parallel to the core between 37 and 43 cm and intersects the left edge of the core near 45 cm. A color gradation over about 0.5 cm, reflecting the presence of a chilled margin, is visible in the basalt between 40 and 45 cm. A large calcite vein cuts both basalt and breccia between 34 and 37 cm.

between about 110 and 90 mbsf in Hole 879A. Within the volcanic and clay-rich facies of the basal carbonate platform (Lithologic Subunits ID and IE) and the underlying weathered volcanic breccia (Lithologic Unit II), the varying mineralogic composition played the dominant role in controlling fluctuations. Because of the enlarged borehole diameter within the carbonate platform facies, resistivity measurements depend on the depth of penetration of the different resistivity sondes; we consider that the medium-penetration resistivity measurements provide the more reliable values and detail (see “Explanatory Notes” chapter, this volume). The FMS imagery was not processed in time for this volume, but we expect that it will show that many of the short-wavelength features have internal complexity, such as groupings of thin beds or irregular patterns of cementation, whereas the distinct resistivity spikes are caused by well-cemented horizons.

### Main Carbonate Platform

#### Lithologic Subunits IA–IC

Interval: Cores 144-879A-1R through -15R  
Assigned depth from logs: 0–149.5 mbsf  
Age: late Aptian to Albian

The upper surface of the carbonate platform was observed to be coated with a dark material in the vibration-isolated television (VIT) survey. This uppermost layer was not recovered during coring, so we attempted to obtain its natural gamma-ray radiation signature through the drill pipe. No significant variation in natural gamma-ray radiation was seen in this interval; therefore, the crust does not contain a major uranium-enrichment associated with a phosphate-rich layer, as was observed on Limalok Guyot (see “Downhole Measurements and Seismic Stratigraphy” section, “Site 871” chapter, this volume).

The main carbonate platform, from the highest significant influx of clay (thorium-rich) at 149.5 mbsf, to the upper limit of reliable geophysical logging measurements at 40.5 mbsf, can be divided into four zones with distinctive resistivity and natural gamma-ray characteristics.

The zone from approximately 40.5 to 100 mbsf has relatively constant medium resistivity (averaging 2–3  $\Omega$ m) and low levels of natural gamma rays (low uranium levels). Variations from the mean resistivity are minor, implying that interbedding of facies is not significant. Only 65 cm was recovered from this 60-m interval (Cores 144-879A-11R through -6R), but these pieces suggest that this zone is dominated by skeletal packstone.

The zone from 100 to 115 mbsf has relatively low resistivity (generally less than 1  $\Omega$ m) and very low levels of natural gamma rays. Previous studies have shown a progressive increase in density and resistivity from grainstone facies through packstone and wackestone to mudstone facies (e.g., Asquith, 1979; Dorfman et al., 1990), therefore, one possibility is that this low-resistivity zone is a grainstone that has high porosity. There was no recovery from this 15-m interval. Core 144-879A-12R (102–112 mbsf) had a rapid drilling penetration rate of only 3 min for the 9.7 m. During the FMS runs, the tool string was partially pulled from its 10° slanting orientation of the borehole to a more upright 8° within this widened interval, and pad contact was lost. Therefore, one possibility is that this zone is caused by its cavernous porosity within the carbonate platform; alternatively, this interval may have been “washed out” during coring.

The zone from 136.5 to 115 mbsf has high resistivity (averaging 5 to 15  $\Omega$ m) in the lower part, followed by a gradual transition to the

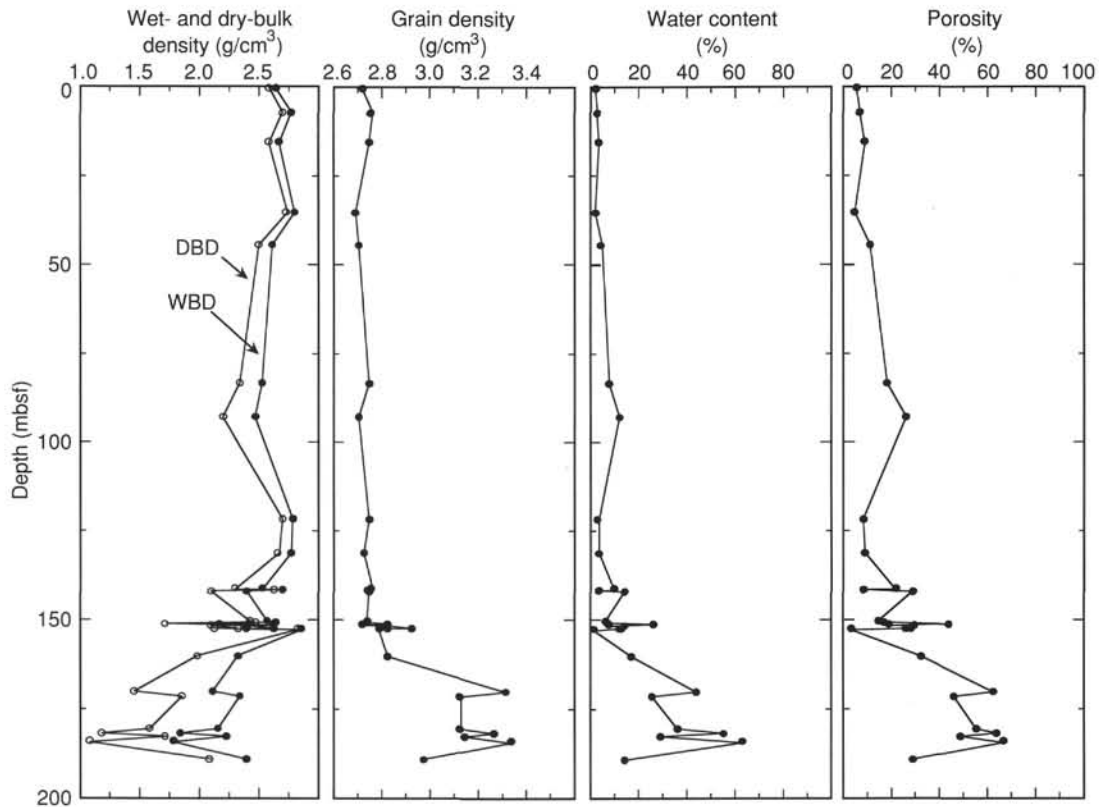


Figure 25. Measurements of index properties (wet- and dry-bulk density, grain density, water content, and porosity) vs. depth, Hole 879A.

low resistivity of the overlying "grainstone" zone. Superimposed on this general trend are several high-amplitude resistivity peaks and troughs, indicating variable degrees of cementation and lime mud content. The general relationship between resistivity and carbonate facies implies that this zone has a much higher content of lime mud than do overlying zones. Recovery from corresponding Core 144-879A-15R through lower Core 144-879A-13R displays a variety of carbonate facies, from gastropod-rich wackestone to rudist floatstone, although only the lower portion of this 21-m-thick zone had significant recovery. Natural gamma-ray radiation in this interval is higher than in overlying zones, averaging about 8 API units.

The lowest zone (from 136.5 to 149.5 mbsf) is characterized by a combination of high natural gamma ray, averaging 10 to 20 API units, caused by high uranium levels, and fairly constant high resistivity, averaging 5 to 6 Wm. This 13-m zone is approximately equivalent to Lithologic Subunit IC (Core 144-879A-16R) of interbedded grayish yellow and dark gray, bioturbated skeletal wackestone. Several peaks appear in the natural gamma rays, with a major event (50 API units) caused by a concentration of uranium at 145.5 to 145.6 mbsf. These uranium concentrations are not associated with resistivity changes, suggesting that redox-front precipitation, rather than enrichment from condensation, may play a major part. We suggest that the uranium enrichments are probably associated with the apparent alternation of oxygenation levels.

#### Interbedded Carbonate and Detrital Volcaniclastics

##### Lithologic Subunits ID-IE

Interval: Cores 144-879A-17R through -10R  
Assigned depth from logs: 149.5–165 mbsf  
Age: late Aptian

This 15-m interval is characterized by four multimeter zones of thorium enrichment. Each of these zones also has decreased resistivity relative to the low-thorium interbeds. These characteristics indicate the presence of clay-rich zones within the host facies. From Cores 144-879A-17R and -18R, dark gray clayey sandstone with volcanic grains and volcanic conglomerates interbedded in clayey limestone to calcareous sandstone was recovered. The uppermost clay-rich interval was considered to be a distinct subunit (Lithologic Subunit ID), but the other levels of thorium-enriched, low-resistivity facies indicates that at least four clay-rich zones exist.

#### Claystone

##### Lithologic Unit II

Interval: Cores 144-879A-19R to upper -21R  
Assigned depth from logs: 165–191 mbsf  
Age: indeterminate

This 26-m interval has constant low resistivity (2–3  $\Omega$ m), high thorium content, and a widened borehole. These characteristics indicate a clay-rich facies. Core recovery from this interval was dominated by reddish to black claystone to weathered volcanic breccia.

#### Basalt

##### Lithologic Unit III

Interval: lower Cores 144-879A-21R through -24R  
Assigned depth from logs and drilling: 191–226.5 mbsf  
Age: indeterminate

Only the upper portion of the basalt complex was logged. The basalt flows, volcanic breccias, and weathering horizons produced very high

Table 8. Index properties data, Hole 879A.

| Core, section, interval (mbsf) | Depth (mbsf) | Wet-bulk density (g/cm <sup>3</sup> ) | Dry-bulk density (g/cm <sup>3</sup> ) | Grain density (g/cm <sup>3</sup> ) | Porosity (%) | Water content (% dry wt) | Void ratio |
|--------------------------------|--------------|---------------------------------------|---------------------------------------|------------------------------------|--------------|--------------------------|------------|
| 144-879A-                      |              |                                       |                                       |                                    |              |                          |            |
| 1R-1, 23-25                    | 0.23         | 2.64                                  | 2.58                                  | 2.72                               | 5.60         | 2.20                     | 0.06       |
| 2R-1, 118-122                  | 7.18         | 2.76                                  | 2.69                                  | 2.76                               | 7.10         | 2.70                     | 0.08       |
| 3R-1, 11-14                    | 15.61        | 2.67                                  | 2.58                                  | 2.75                               | 9.00         | 3.60                     | 0.10       |
| 5R-1, 61-63                    | 35.21        | 2.79                                  | 2.73                                  | 2.69                               | 5.10         | 1.90                     | 0.05       |
| 6R-1, 16-19                    | 44.46        | 2.61                                  | 2.49                                  | 2.71                               | 11.40        | 4.70                     | 0.13       |
| 10R-1, 28-30                   | 83.18        | 2.53                                  | 2.34                                  | 2.75                               | 18.30        | 8.00                     | 0.22       |
| 11R-1, 11-17                   | 92.61        | 2.47                                  | 2.20                                  | 2.71                               | 26.40        | 12.30                    | 0.36       |
| 14R-1, 21-25                   | 121.71       | 2.78                                  | 2.70                                  | 2.75                               | 8.40         | 3.20                     | 0.09       |
| 15R-1, 17-22                   | 131.27       | 2.76                                  | 2.66                                  | 2.73                               | 9.10         | 3.50                     | 0.10       |
| 16R-1, 64-66                   | 141.44       | 2.53                                  | 2.30                                  | 2.76                               | 21.80        | 9.70                     | 0.28       |
| 16R-1, 98-101                  | 141.78       | 2.70                                  | 2.62                                  | 2.74                               | 8.40         | 3.30                     | 0.09       |
| 16R-1, 136-139                 | 142.16       | 2.40                                  | 2.10                                  | 2.75                               | 29.00        | 14.10                    | 0.41       |
| 17R-1, 6-8                     | 150.46       | 2.57                                  | 2.42                                  | 2.74                               | 15.20        | 6.40                     | 0.18       |
| 17R-1, 47-49                   | 150.87       | 2.64                                  | 2.47                                  | 2.74                               | 17.00        | 7.10                     | 0.20       |
| 17R-1, 80-82                   | 151.20       | 2.17                                  | 1.72                                  | 2.83                               | 44.00        | 26.20                    | 0.78       |
| 17R-1, 97-102                  | 151.37       | 2.63                                  | 2.43                                  | 2.72                               | 19.00        | 8.00                     | 0.23       |
| 17R-1, 123-125                 | 151.63       | 2.40                                  | 2.10                                  | 2.82                               | 29.70        | 14.50                    | 0.42       |
| 17R-2, 45-47                   | 152.35       | 2.63                                  | 2.33                                  | 2.93                               | 28.60        | 12.50                    | 0.40       |
| 17R-2, 57-58                   | 152.47       | 2.40                                  | 2.12                                  | 2.83                               | 26.70        | 12.90                    | 0.36       |
| 17R-2, 77-79                   | 152.67       | 2.85                                  | 2.82                                  | 2.79                               | 3.40         | 1.20                     | 0.03       |
| 18R-1, 30-32                   | 160.40       | 2.32                                  | 1.98                                  | 2.83                               | 32.70        | 16.90                    | 0.49       |
| 19R-1, 32-35                   | 170.02       | 2.11                                  | 1.46                                  | 3.32                               | 62.70        | 43.90                    | 1.68       |
| 19R-2, 61-63                   | 171.63       | 2.34                                  | 1.86                                  | 3.13                               | 46.50        | 25.60                    | 0.87       |
| 20R-1, 108-110                 | 180.48       | 2.15                                  | 1.58                                  | 3.13                               | 55.70        | 36.00                    | 1.26       |
| 20R-2, 123-126                 | 181.97       | 1.84                                  | 1.18                                  | 3.27                               | 64.20        | 55.60                    | 1.79       |
| 20R-3, 49-52                   | 182.73       | 2.22                                  | 1.72                                  | 3.15                               | 49.10        | 29.30                    | 0.96       |
| 20R-4, 50-53                   | 184.24       | 1.78                                  | 1.09                                  | 3.34                               | 67.10        | 63.10                    | 2.04       |
| 21R-1, 35-37                   | 189.05       | 2.39                                  | 2.09                                  | 2.98                               | 29.50        | 14.50                    | 0.42       |

resistivity values, averaging about 7  $\Omega$ m, with several meter-scale peaks exceeding 10  $\Omega$ m. Natural gamma-ray intensity remains high (about 30 API units), with only minor fluctuations.

### Downhole Magnetometer Measurements

A three-axis fluxgate magnetometer is part of the FMS tool string. Data about the orientation and strength of the magnetic field within the borehole were collected at 15-cm (0.50 ft) intervals, in contrast to the 2.5-mm sampling rate of the FMS resistivity image data. The three-component magnetic data (the horizontal "x" component parallel to the FMS Pad 1 direction, the horizontal "y" component perpendicular to the Pad 1 direction, and the vertical "z" component) enable us to calculate the horizontal and vertical intensities, inclination, and relative declination of the magnetic field with depth. The magnetic direction is used to orient the FMS traces with respect to magnetic north. Within rocks having a strong natural remanent magnetization (NRM) that is different in direction than the present-day magnetic field, the FMS orientation will be slightly distorted, but we acquire valuable information about the NRM directions of the magnetization within those rocks (Fig. 27).

Post-cruise analysis, including calculations based on a disk geometry, will be necessary to model these magnetic field observations by using alternating normal and reversed magnetization and variable NRM intensities of different layers (e.g., Pozzi et al., 1988; Gallet and Courtillot, 1989; Hamano and Kinoshita, 1990).

### Seismic Stratigraphy

Single-channel seismic profiles were obtained during four crossings of Site 879 before occupation of the site. The first used a 200-in.<sup>3</sup> water gun as a sound source, and the next three used an 80-in.<sup>3</sup> water gun. These data were recorded on a Masscomp computer, filtered, and redisplayed. The last crossing, using an 80-in.<sup>3</sup> water gun and during which a beacon was dropped, is displayed in Figure 5. These data are not of high quality, and sub-bottom reflections are virtually invisible. As such, these data were barely adequate for selecting a drill site, but they are superior to profiles that had been obtained before Leg 144. The data in Figure 5 show a vague sub-bottom reflector at about 0.2 s TWT below the seafloor.

## SUMMARY AND CONCLUSIONS

A very preliminary interpretation of the cores obtained at Site 879 suggests that the upper portion of the volcanic edifice shows evidence of basaltic intrusion into wet sediments, as documented by the peperite. This is overlain by a thin layer of yellowish volcanic breccia that appears to have undergone intense weathering. A high-energy marine and/or nonmarine environment (beach and/or stream) eroded and rounded the pebbles of the basalt to form the conglomerate. These highly vesicular, aphyric basalt pebbles are weathered to orange and yellowish brown. Another breccia containing basalt clasts with a red clay and volcanic sand matrix has undergone extensive oxidation, probably as the result of subaerial weathering.

By the late Aptian, flooding of the weathered volcanic edifice by marine waters is documented by the calcareous nature and presence of biotic contents in the rudstone, calcareous sandstone, and argillaceous limestone. Progressive and periodic flooding of this former island are documented by lagoonal deposits with nerineids to more open-marine deposits containing planktonic organisms. The presence of coal and wood associated with the beginning of the shallow-water marine deposition, as well as with the basaltic lithoclasts, attests to the terrestrial influence at this site. This implies that a vegetated, exposed volcanic edifice was close to Site 879. Moreover, the presence of coal contained within the sandstone, in addition to well-rounded basalt pebbles and molluscan molds in the matrix of the volcanic conglomerate, are consistent with deposition in a near-shore marine environment. The argillaceous limestone is heavily bioturbated, which potentially indicates oxygenated bottom-water conditions. The upward decrease of terrestrial influence, as suggested by a progressive decrease in the abundance of plant remains and volcanic grains until they are absent, parallels the establishment of more open-marine conditions. Planktonic foraminifers are present in the middle of the carbonate sequence and record periods of maximum flooding. These pelagic deposits are heavily bioturbated, indicating oxygenated bottom-water conditions.

A low-energy, shallow-marine environment follows at this location, as shown by the presence of lime mud in the packstone and wackestone, with rare grainstone intervals, as well as by the biotic contents of oysters and nerineids. This low-energy environment gradually evolved into a more open-marine, higher energy setting documented by an

oncolite-rich interval and then the presence of coral-molluscan rudstone and floatstone. The carbonate platform subsided into the pelagic realm after possibly middle Albian time.

#### REFERENCES\*

- Asquith, G.D., 1979. *Subsurface Carbonate Depositional Models: A Concise Review*. Tulsa, OK (Petroleum Publ. Co.).
- Dorfman, M.H., Newey, J.-J., and Coates, G.R., 1990. New techniques in lithofacies determination and permeability prediction in carbonates using well logs. In Hurst, A., Lovell, M.A., and Morton, A.C. (Eds.), *Geological Applications of Wireline Logs*. Geol. Soc. Spec. Publ. London, 48:113–120.
- Gallet, Y., and Courtillot, V., 1989. Modeling magnetostratigraphy in a borehole. *Geophysics*, 54:973–983.
- Hamano, Y., and Kinoshita, H., 1990. Magnetization of the oceanic crust inferred from magnetic logging in Hole 395A. In Detrick, R., Honnorez, J., Bryan, W.B., Juteau, T., et al., *Proc. ODP. Sci. Results*, 106/109: College Station, TX (Ocean Drilling Program), 275–281.
- Heezen, B.C., Matthews, J.L., Catalano, R., Natland, J., Coogan, A., Tharp, M., and Rawson, M., 1973. Western Pacific guyots. In Heezen, B.C., MacGregor, I.D., et al., *Init. Repts. DSDP*, 20: Washington (U.S. Govt. Printing Office), 653–723.
- Hydrographer of the Navy, 1991. *Admiralty Tide Tables (Vol. 3): Pacific Ocean and Adjacent Seas*: London (Hydrographer of the Navy).
- Nakanishi, M., Tamaki, K., and Kobayashi, K., 1992. Magnetic anomaly lineations from Late Jurassic to Early Cretaceous in the west-central Pacific Ocean. *Geophys. J. Int.*, 109:701–719.
- , 1992. A new Mesozoic isochron chart of the northwestern Pacific Ocean: paleomagnetic and tectonic implications. *Geophys. Res. Lett.*, 19:693–696.
- Ozima, M., Kaneoka, I., and Ujje, H., 1977.  $^{40}\text{Ar}$ - $^{39}\text{Ar}$  age of rocks, and development mode of the Philippine Sea. *Nature*, 267:816–818.
- Pozzi, J.-P., Martin, J.P., Pocachard, J., Feinberg, H., and Galdeano, A., 1988. In situ magnetostratigraphy: interpretation of magnetic logging in sediments. *Earth Planet. Sci. Lett.*, 88:357–373.
- Sager, W.W., Duncan, R.A., and Handschumacher, D.W., in press. Paleomagnetism of the Japanese and Marcus-Wake seamounts, Western Pacific Ocean. In Pringle, M.S., Sager, W.W., Sliter, W.V., and Stein, S. (Eds.), *The Mesozoic Pacific*. Am. Geophys. Union, Geophys. Monogr. Ser.
- van Waasbergen, R.J., and Winterer, E.L., in press. Summit geomorphology of Western Pacific guyots. In Pringle, M.S., Sager, W.W., Sliter, W.V., and Stein, S. (Eds.), *The Mesozoic Pacific*. Am. Geophys. Union, Geophys. Monogr. Ser.
- Vogt, P.R., and Smoot, N.C., 1984. The Geisha Guyots: multibeam bathymetry and morphometric interpretation. *J. Geophys. Res.*, 89:11085–11107.

\* Abbreviations for names of organizations and publication titles in ODP reference lists follow the style given in *Chemical Abstracts Service Source Index* (published by American Chemical Society).

Ms 144IR-112

**NOTE: For all sites drilled, core-description forms (“barrel sheets”) and core photographs can be found in Section 3, beginning on page 453. Conventional log, FMS, dipmeter, and geochemical log (element and oxide weight %) data can be found in CD-ROM form (back pocket).**

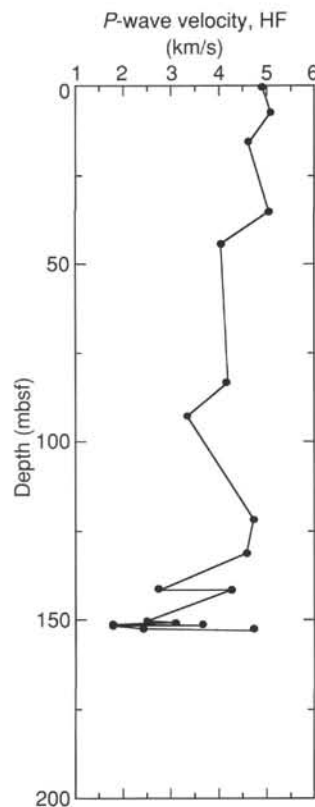


Figure 26. Hamilton Frame (HF) measurements of compressional wave velocity vs. depth, Hole 879A.

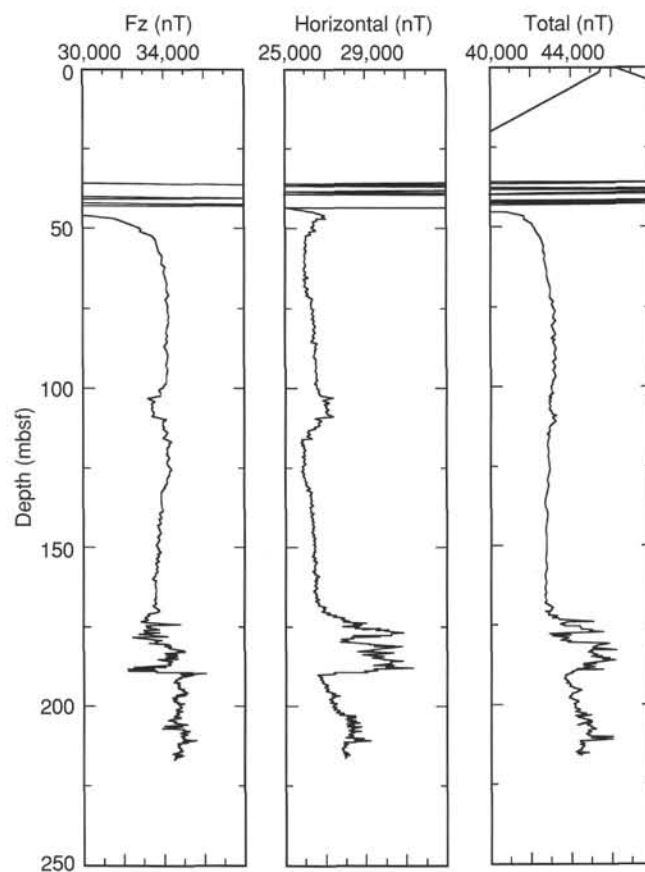


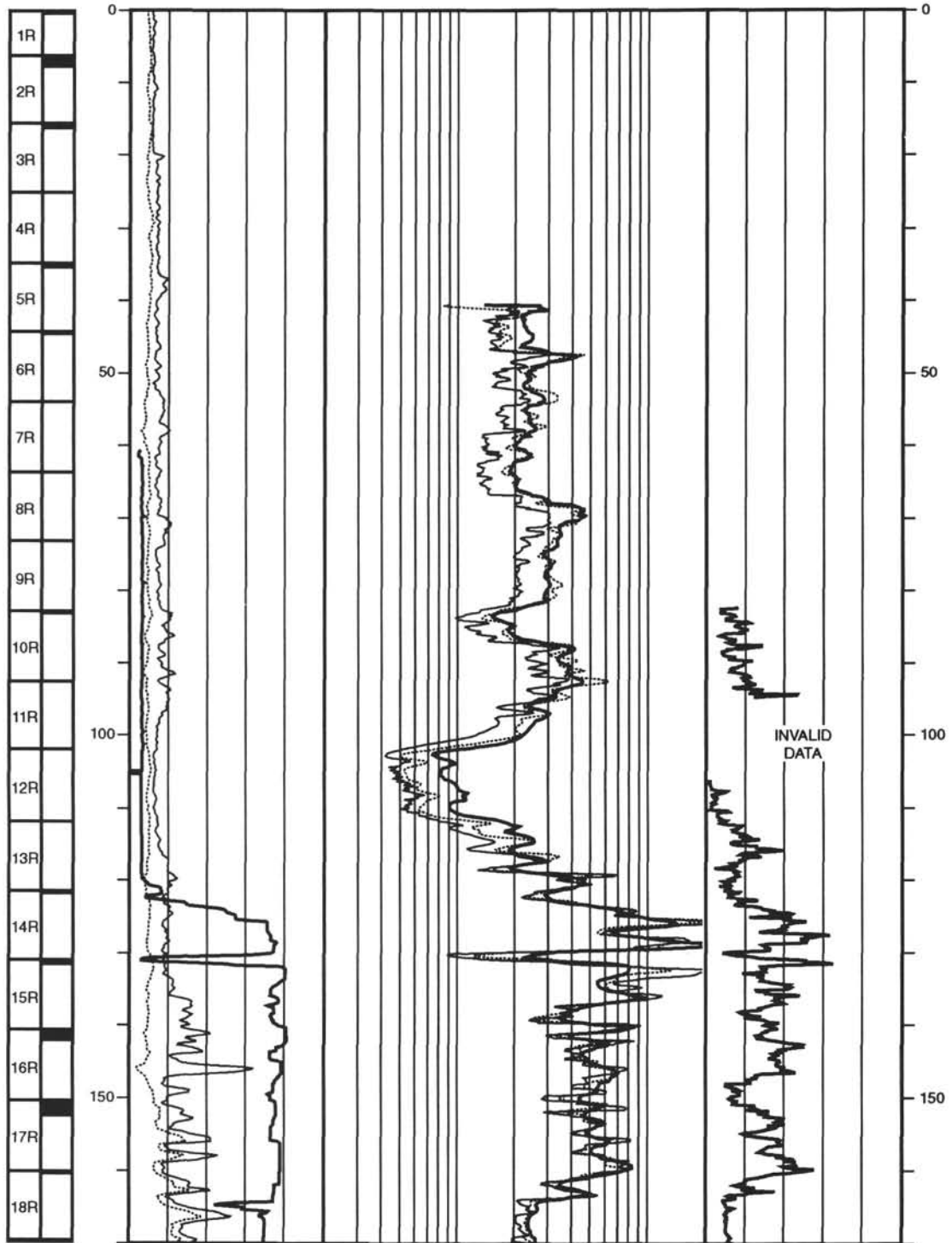
Figure 27. Variation of the magnetic field obtained by the Formation MicroScanner (FMS) three-axis fluxgate magnetometer instrument (GPIT, Hole 879A, Run 2). The three-component magnetic data (FX is the horizontal "x" component, parallel to the FMS Pad 1 direction; FY is the horizontal "y" component, perpendicular to the FMS Pad 1 direction; and FZ is the vertical "z" component) enable one to calculate horizontal intensity, inclination, and relative declination.

**Table 9. Hamilton Frame measurements of compressional wave velocity, Hole 879A.**

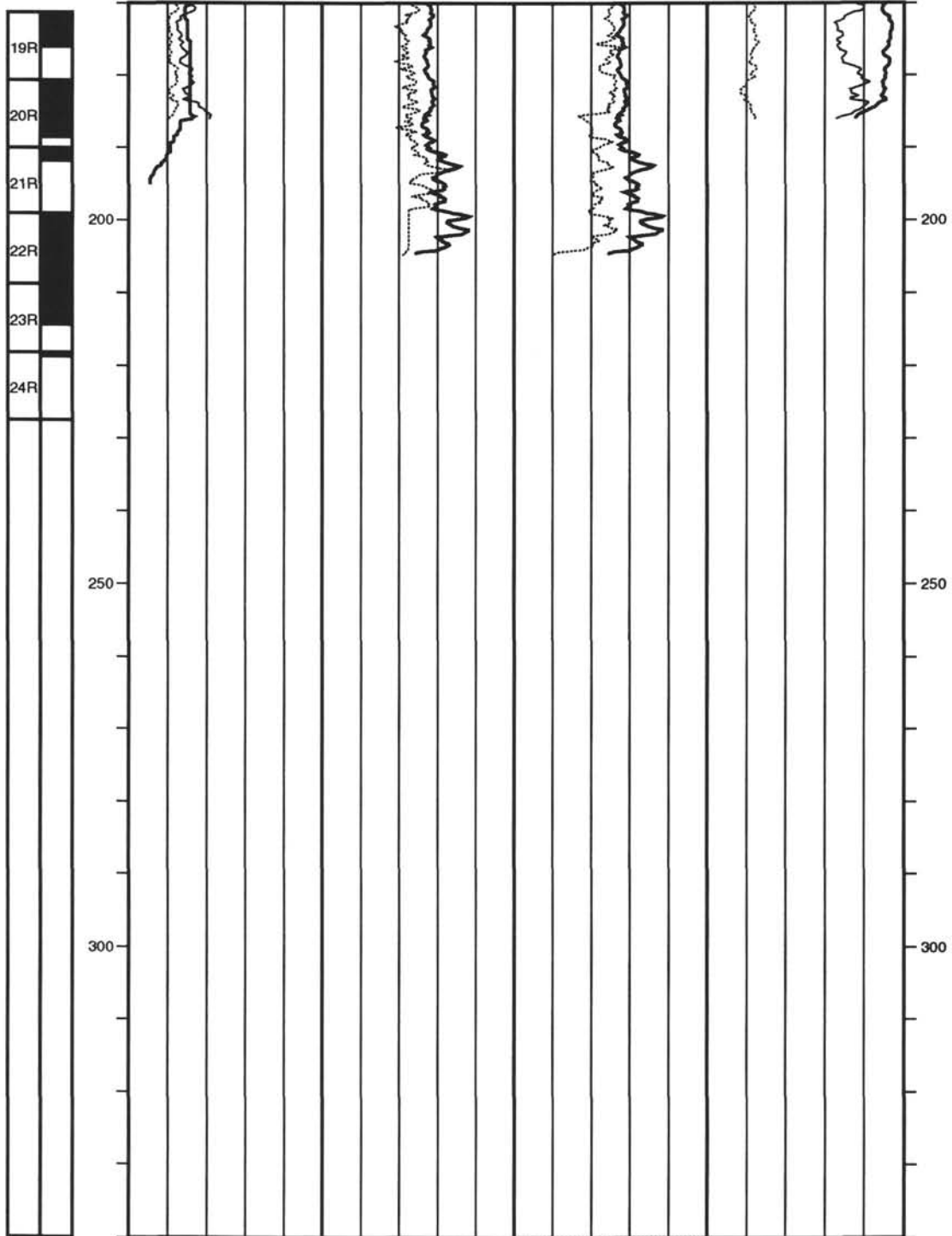
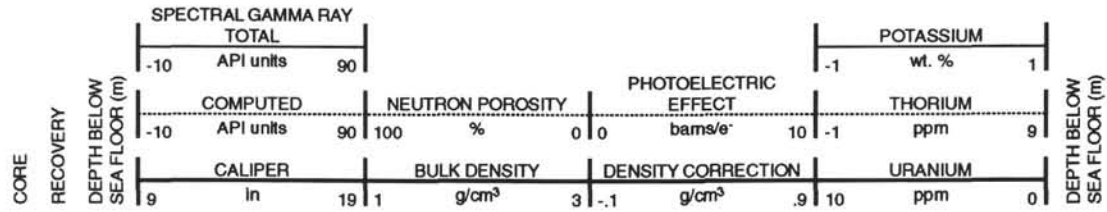
| Core, section, interval (cm) | Depth (mbsf) | Distance (mm) | Corrected travelttime ( $\mu$ s) | Measured velocity (m/s) |
|------------------------------|--------------|---------------|----------------------------------|-------------------------|
| 144-879A-                    |              |               |                                  |                         |
| 1R-1, 23-25                  | 0.23         | 18.94         | 6.85                             | 4919.48                 |
| 2R-1, 118-122                | 7.18         | 17.05         | 6.35                             | 5089.55                 |
| 3R-1, 11-14                  | 15.61        | 17.37         | 6.75                             | 4632.00                 |
| 5R-1, 61-63                  | 35.21        | 16.74         | 6.32                             | 5042.17                 |
| 6R-1, 16-19                  | 44.46        | 9.44          | 5.32                             | 4068.97                 |
| 10R-1, 28-30                 | 83.18        | 21.18         | 8.06                             | 4185.77                 |
| 11R-1, 11-17                 | 92.61        | 11.84         | 6.53                             | 3354.11                 |
| 14R-1, 21-25                 | 121.71       | 11.97         | 5.52                             | 4750.00                 |
| 15R-1, 17-22                 | 131.27       | 21.03         | 7.58                             | 4591.70                 |
| 16R-1, 64-66                 | 141.44       | 20.79         | 10.53                            | 2760.96                 |
| 16R-1, 98-101                | 141.78       | 15.58         | 6.65                             | 4268.49                 |
| 17R-1, 6-8                   | 150.46       | 13.79         | 8.53                             | 2493.67                 |
| 17R-1, 47-49                 | 150.87       | 21.33         | 9.91                             | 3086.83                 |
| 17R-1, 80-82                 | 151.20       | 12.63         | 10.10                            | 1778.87                 |
| 17R-1, 97-102                | 151.37       | 19.47         | 8.29                             | 3680.53                 |
| 17R-1, 123-125               | 151.63       | 15.52         | 11.67                            | 1790.08                 |
| 17R-2, 45-47                 | 152.35       | 21.30         | 11.83                            | 2412.23                 |
| 17R-2, 77-79                 | 152.67       | 13.88         | 5.92                             | 4753.43                 |

Hole 879A: Resistivity-Velocity-Natural Gamma Ray Log Summary

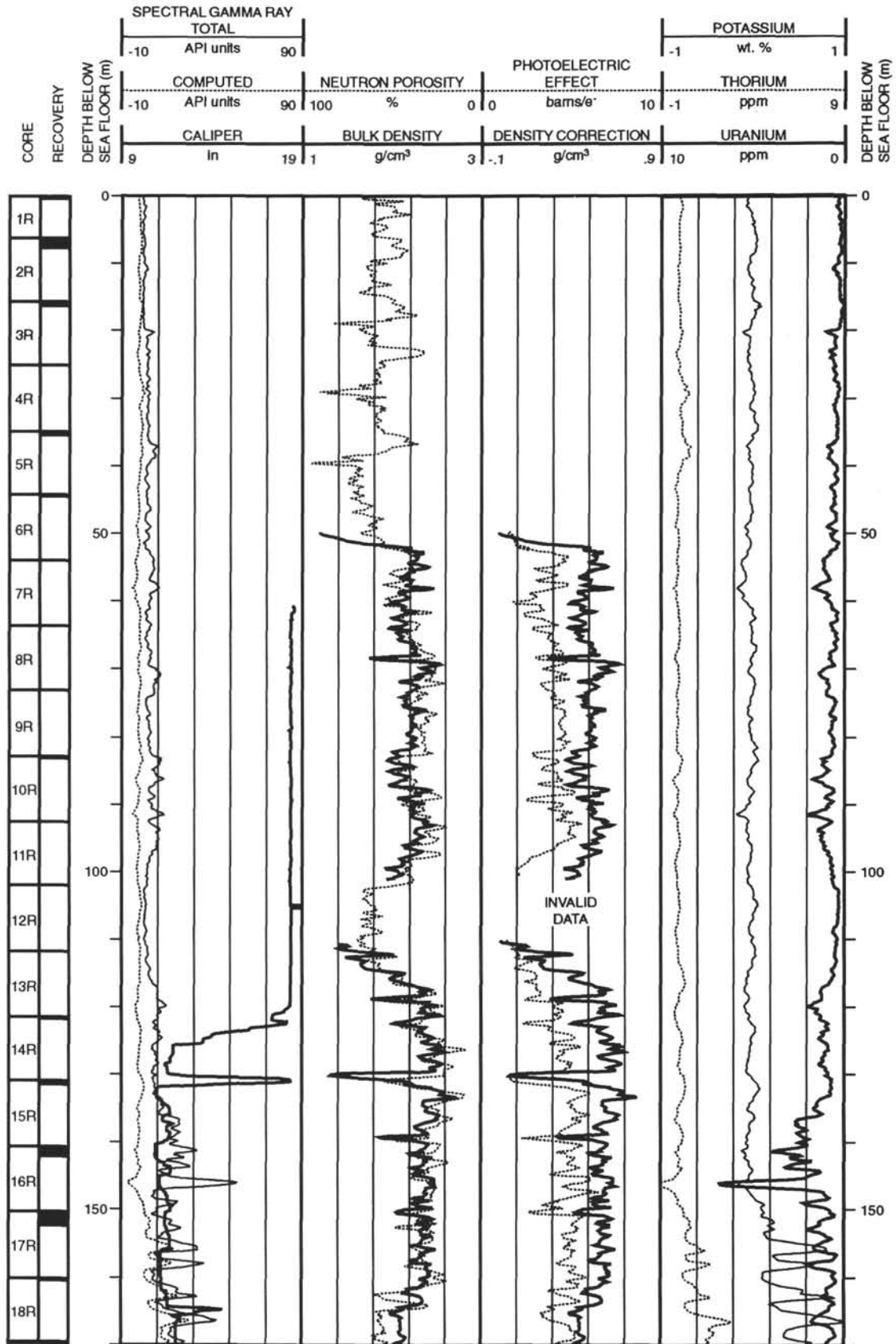
| CORE RECOVERY | SPECTRAL GAMMA RAY |           |    |       | RESISTIVITY |     |          |     | DEPTH BELOW SEA FLOOR (m) |
|---------------|--------------------|-----------|----|-------|-------------|-----|----------|-----|---------------------------|
|               | TOTAL              |           |    |       | FOCUSED     |     |          |     |                           |
|               | -10                | API units | 90 | .2    | ohm-m       | 20  |          |     |                           |
|               | COMPUTED           |           |    |       | MEDIUM      |     |          |     | DEPTH BELOW SEA FLOOR (m) |
| -10           | API units          | 90        | .2 | ohm-m | 20          |     |          |     |                           |
|               | CALIPER            |           |    |       | DEEP        |     | VELOCITY |     | DEPTH BELOW SEA FLOOR (m) |
| 19            | in                 | 9         | .2 | ohm-m | 20          | 1.5 | km/s     | 6.5 |                           |



Hole 879A: Density-Porosity-Natural Gamma Ray Log Summary (continued)



Hole 879A: Density-Porosity-Natural Gamma Ray Log Summary



Hole 879A: Resistivity-Velocity-Natural Gamma Ray Log Summary (continued)

| CORE RECOVERY | SPECTRAL GAMMA RAY |           |    |    | RESISTIVITY |    |          |      | DEPTH BELOW SEA FLOOR (m) |
|---------------|--------------------|-----------|----|----|-------------|----|----------|------|---------------------------|
|               | TOTAL              |           |    |    | FOCUSED     |    |          |      |                           |
|               | -10                | API units | 90 | .2 | ohm-m       | 20 |          |      |                           |
|               | COMPUTED           |           |    |    | MEDIUM      |    |          |      |                           |
|               | -10                | API units | 90 | .2 | ohm-m       | 20 |          |      |                           |
|               | CALIPER            |           |    |    | DEEP        |    | VELOCITY |      |                           |
|               | 19                 | in        | 9  | .2 | ohm-m       | 20 | 1.5      | km/s | 6.5                       |

